JGR Oceans

RESEARCH ARTICLE
10.1029/2022JC018971

The Influence of Agulhas Leakage on Primary Production and Nitrogen Cycling in the Southeastern Atlantic Ocean

Sina Wallschuss[1], Mhlangabezi Mdutyana[1,2], Ruan G. Parrott[1], Heather J. Forrer[3], Raymond Roman[1], David R. Walker[4], Isabelle J. Ansorge[1], and Sarah E. Fawcett[1,5]

[1]Department of Oceanography, University of Cape Town, Cape Town, South Africa, [2]Southern Ocean Carbon and Climate Observatory (SOCCO), CSIR, Cape Town, South Africa, [3]Department of Earth, Ocean, and Atmospheric Science, Florida State University, Tallahassee, FL, USA, [4]Department of Conservation and Marine Sciences, Cape Peninsula University of Technology, Cape Town, South Africa, [5]Marine and Antarctic Research Center for Innovation and Sustainability (MARIS), University of Cape Town, Cape Town, South Africa

Abstract The well-established importance of Agulhas Current "leakage" for Indian-Atlantic Ocean exchange of heat and salt raises the question of the relevance of Agulhas eddies for carbon and nitrogen cycling. We measured net primary production (NPP), nitrate and ammonium uptake, and nitrification along a transect of the Cape Basin (CB) in winter 2017, including across an anticyclonic Agulhas eddy sampled at high-resolution. Euphotic zone-integrated rates of NPP and nitrogen uptake were more than three-fold lower at the eddy center than at its edges, with intermediate rates measured outside the eddy. Additionally, proportionally more nitrate was consumed at the eddy edges than at its center. Mixed-layer integrated nitrification rates were highest at the eddy-center, with lower rates at the edges and in the surrounding basin. Accounting for phytoplankton consumption of newly nitrified nitrate in the eddy decreased the carbon export potential inferred from nitrate uptake (i.e., the *f*-ratio) by 66% ± 37% (vs. a 14% ± 22% decrease across the rest of the transect). At most stations, NPP and total measured nitrogen uptake were decoupled relative to stoichiometric expectations, with roughly a third of NPP possibly supported by regenerated dissolved organic nitrogen (DON). Accounting for DON uptake decreased the average *f*-ratio from 0.28 ± 0.26 to 0.22 ± 0.21, with the highest *f*-ratio estimated for an eddy-edge station (0.64) and the lowest for its center (0.00). While the low productivity metrics measured in the eddy-center could imply that Agulhas leakage decreases carbon export potential in the CB, enhanced nutrient supply and consumption at eddy edges may (partly) offset this reduction.

Plain Language Summary Mesoscale eddies are abundant in the ocean, transporting physical, chemical, and biological properties from the eddy source region. Eddies can also cause small-scale upwelling and/or downwelling, which affect the local biogeochemistry and biology (e.g., altering phytoplankton growth by changing the nutrient and/or light conditions). Large anticyclonic eddies that pinch off the Agulhas Current south of Africa transfer warm, salty waters from the Indian to the Atlantic Ocean, thereby playing a crucial role in ocean circulation. By contrast, little is known of the role of Agulhas eddies in carbon and nitrogen cycling. We find that the physical perturbations caused by the passage of an Agulhas eddy into the southeastern Atlantic stimulate primary production and nitrate uptake at the eddy edges, implying enhanced CO_2 removal to depth, while productivity (and CO_2 removal) is depressed at the eddy center. Additionally, the deep mixed layers created by the eddy's anticyclonic circulation favor high rates of nitrification, which produces recycled nitrate. Phytoplankton consumption of this nitrate yields no net removal of CO_2, exacerbating the dampening effect of the eddy on Atlantic productivity. It is possible, however, that the reduction in productivity may be partly offset by the elevated supply and consumption of subsurface nutrients at the eddy edges.

Key Points:

- Primary production and carbon export potential are elevated at Agulhas eddy edges and reduced at their centers
- Agulhas eddies host high rates of mixed-layer nitrification that can supply 100% of phytoplankton nitrate
- Dissolved organic nitrogen appears to fuel a significant fraction of primary production in Agulhas eddies and the Cape Basin

Supporting Information:

Supporting Information may be found in the online version of this article.

Correspondence to:

S. Wallschuss,
wllsin005@myuct.ac.za

Citation:

Wallschuss, S., Mdutyana, M., Parrott, R. G., Forrer, H. J., Roman, R., Walker, D. R., et al. (2022). The influence of Agulhas leakage on primary production and nitrogen cycling in the southeastern Atlantic Ocean. *Journal of Geophysical Research: Oceans*, *127*, e2022JC018971. https://doi.org/10.1029/2022JC018971

Received 10 JUN 2022
Accepted 5 SEP 2022

Author Contributions:

Conceptualization: Sina Wallschuss, Sarah E. Fawcett
Data curation: Sina Wallschuss, Ruan G. Parrott, Heather J. Forrer, Raymond Roman, David R. Walker
Formal analysis: Sina Wallschuss, Mhlangabezi Mdutyana, Sarah E. Fawcett
Funding acquisition: Sarah E. Fawcett
Investigation: Sina Wallschuss, Sarah E. Fawcett
Methodology: Sina Wallschuss, Mhlangabezi Mdutyana, Ruan G. Parrott, David R. Walker, Sarah E. Fawcett
Project Administration: Sina Wallschuss, Sarah E. Fawcett

1. Introduction

The Agulhas Current is the strongest western boundary current on Earth (Bryden et al., 2005) transporting 84 ± 11 Sv of warm (sub)tropical water into the mid-latitudes annually (Beal et al., 2015). Its path is guided by the southern African continental shelf (Duncombe Rae, 1991), from which the current separates at the southernmost tip. Beyond this, the current retroflects back into the Indian Ocean basin to form the eastward-flowing Agulhas Return Current by means of a tight anticlockwise loop termed the Agulhas Retroflection (Bang, 1970; Lutjeharms & van Ballegooyen, 1984). A portion of Agulhas Current flow escapes at the retroflection, entering the South Atlantic as large Agulhas rings and smaller eddies and filaments (Gordon et al., 1987; Lutjeharms &

Resources: Sina Wallschuss, Sarah E. Fawcett
Supervision: Sarah E. Fawcett
Visualization: Sina Wallschuss, Sarah E. Fawcett
Writing – original draft: Sina Wallschuss, Sarah E. Fawcett
Writing – review & editing: Mhlangabezi Mdutyana, Ruan G. Parrott, Heather J. Forrer, Raymond Roman, Sarah E. Fawcett

Cooper, 1996; Lutjeharms & van Ballegooyen, 1988). Collectively, these features are termed Agulhas "leakage" (Lutjeharms, 2006) and are estimated to transport 10–20 Sv of Indian Ocean water into the Atlantic annually (Beal et al., 2011; Holton et al., 2017; Richardson, 2007), with a recent estimate of 21.3 ± 4.7 Sv/yr (Daher et al., 2020).

Agulhas leakage is a key component of the upper limb of the South Atlantic meridional overturning circulation (SAMOC) and thus, the greater global MOC, providing the primary transport mechanism for heat and salt between the Indian and South Atlantic basins (Donners & Drijfhout, 2004; Gordon et al., 1992). Agulhas rings and eddies are generated when the Agulhas Retroflection loop periodically sheds anticyclonically circulating vortices of relatively warm water (Gordon et al., 1987; Lutjeharms, 1981; Lutjeharms & Gordon, 1987) that facilitate inter-ocean transport by encapsulating and transferring south Indian Ocean thermocline and intermediate waters to the South Atlantic (Gordon, 1985; Gordon et al., 1992). Averaging 240 ± 40 km in diameter (Duncombe Rae, 1991) and at times extending to the sea floor (van Aken et al., 2003). Agulhas rings are twice as energetic as any other eddy in the global ocean (Olson & Evans, 1986) and strongly perturb an otherwise stratified and nutrient-deplete South Atlantic gyre (Dufois et al., 2016). The frequency of ring-shedding events is debated but estimates converge on four to six times a year (De Ruijter et al., 1999; Gordon et al., 1992; Richardson, 2007).

Agulhas rings and eddies are generally longer-lived than other ocean eddies. Their injection into the mean westerly flow of the South Atlantic and their self-induced motion carries them away from the retroflection region (Byrne et al., 1995; Olson & Evans, 1986), with some observed to persist for months near the retroflection and for years in the South Atlantic gyre and beyond (e.g., Byrne et al., 1995; Lehahn et al., 2011; McDonagh & Heywood, 1999). The main control on Agulhas leakage is the strength and position of the wind field over the Indian Ocean (Beal et al., 2011). However, Agulhas leakage characteristics and variability are also determined by flow instabilities, interactions with local bathymetry, and other nonlinear mesoscale (10–100 km in the horizontal) dynamics (De Ruijter et al., 1999; Speich et al., 2006; Zharkov & Nof, 2008). The net effect is a highly dynamic system (i.e., the "Cape Basin [CB]") that is characterized by elevated spatial and temporal variability (Duncombe Rae et al., 1992). Indeed, the CB is "virtually filled" with cyclonic and anticyclonic eddies that interact constantly (Richardson et al., 2003), making it the region of highest eddy kinetic energy in the world (Boebel et al., 2003; Capuano et al., 2018). The physical perturbations induced by Agulhas leakage may have significant biogeochemical consequences for the otherwise oligotrophic South Atlantic gyre; to-date, however, these remain largely unexplored.

Rings and eddies are abundant and ubiquitous features in the global ocean. They produce turbulent and chaotic flow fields (e.g., Boebel et al., 2003) and appear as "pools" of anomalous conditions as they transport water from their source regions (Provenzale, 1999). During their intensification (i.e., "spin-up") period, cyclonic eddies (cold-cored) dome the pycnocline upward, driving upwelling at their centers. Conversely, anticyclonic eddies (warm-cored) depress the seasonal and main pycnocline, driving localized downwelling (Falkowski et al., 1991; Siegel et al., 1999). Cyclonic eddies have been observed to temporarily boost primary productivity due to eddy pumping of deep nutrients into the euphotic zone at their centers (The Ring Group, 1981). Anticyclonic eddies, by contrast, are expected to be relatively unproductive since downwelling at their centers impedes the upward nutrient supply and yields deep mixed-layers that may cause light limitation of phytoplankton (Lévy et al., 1998, 1999). However, at the edges of anticyclonic eddies, submesoscale (1–10 km in the horizontal) upwelling and mixing can inject nutrients into surface waters. Similarly, eddy-wind interactions can at times drive upward nutrient supply at eddy centers (Flierl & McGillicuddy, 2002; Stern, 1965). Furthermore, during their spin-down period, anticyclonic eddies experience re-stratification, which can also cause upwelling at their centers (Flierl & McGillicuddy, 2002).

In this study, we investigate the effect of Agulhas eddies on the productivity of the southeastern Atlantic Ocean by measuring rates of net primary production (NPP) and nitrogen (N) cycling inside and outside an Agulhas eddy in the CB. NPP quantifies the rate at which phytoplankton convert carbon dioxide (CO_2) to organic carbon biomass and represents the energy available to an ecosystem. The export of some fraction of NPP from the euphotic zone and its sequestration in the deep ocean underpins the ocean's biological pump, which exerts a dominant control on the atmospheric CO_2 concentration (De La Rocha & Passow, 2014; Volk & Hoffert, 1985). The "new production paradigm" provides a framework for quantifying the strength of the biological pump, leveraging the fact that NPP can be fueled by two different N sources, "new" and "regenerated" (Dugdale & Goering, 1967). New N is predominantly supplied to the euphotic zone as an upward flux of subsurface nitrate (NO_3^-), augmented by N_2

fixation and atmospheric N deposition, and supports the fraction of NPP termed "new production." By contrast, regenerated N is produced largely via heterotrophic activity in the euphotic zone and exists mainly as recycled ammonium (NH_4^+) and dissolved organic N (DON) forms such as urea. NPP fueled by regenerated N is termed "regenerated" production. From a mass balance perspective, NPP supported by new N equates to the flux of CO_2 into the deep ocean (i.e., "export production") while regenerated production yields no net removal of CO_2 to depth (Dugdale & Goering, 1967; Eppley & Peterson, 1979). As such, NO_3^--based phytoplankton growth is often used as a proxy for carbon export potential. However, euphotic zone NO_3^- can also be supplied by in situ nitrification, the chemoautotrophic process by which NH_4^+ is oxidized to nitrite (NO_2^-) and then NO_3^-. Phytoplankton growth fueled by this NO_3^- amounts to regenerated rather than new production. Constraining nitrification coincident with measurements of NPP and N uptake is essential for accurately estimating new production and carbon export potential (Yool et al., 2007).

While the physics of the Agulhas Current and its leakage have to-date been heavily studied due to their implications for the SAMOC and global climate (e.g., Beal et al. (2011) and references therein), far less is known of the consequences of leakage for Atlantic biogeochemistry, either due to inter-ocean transport of biological and chemical properties or to the in situ alteration of "background" Atlantic conditions. The central aim of this study is an improved understanding of carbon and N cycling in Agulhas eddies and the surrounding CB. We posit that while productivity may be low in the center of anticyclonic Agulhas eddies, the physical perturbations associated with these features may stimulate both total and new production at their edges, adding to a growing body of evidence that anticyclonic eddies are more productive than was once thought (e.g., Dufois et al., 2014, 2016; McGillicuddy et al., 2007).

2. Materials and Methods

2.1. Site Description and Eddy Tracking

Sampling was carried out aboard the R/V *SA Agulhas II* in July 2017 (VOY026) along a section of the South Atlantic MOC Basin-wide Array (SAMBA; Ansorge et al., 2014) line (17.5°E–0°E along 34.5°S) (Figure 1). Seven conductivity-temperature-depth (CTD) casts were conducted on the outbound leg of the cruise (Stations 1–7) and 17 were deployed on the inbound leg (Stations 8–24) (Table S1 in Supporting Information S1). The primary cruise aim was the refurbishment of current and pressure recording inverted echo sounders moored along the SAMBA line; the biogeochemical stations were thus largely selected opportunistically around the positions of these moorings. Nonetheless, on the inbound leg, we purposefully sampled an Agulhas eddy (E1) at high resolution.

At the time of sampling, E1 was apparent as a positive sea level anomaly (SLA) at ∼13°E (Figure 1b). This eddy was tracked prior to and during the cruise using SLA data (Figure S1 in Supporting Information S1) and the shipboard acoustic doppler current profiler (ADCP) (Figure S2 in Supporting Information S1) (as in Hall and Lutjeharms (2010) and Rubio et al. (2009)). The SLA data were obtained from a global multi-satellite Delayed-time Absolute Dynamic Topography (1/4° resolution) gridded L4 product, produced by the SSALTO/DUACS and made available by the European Copernicus Marine Environment Monitoring Service (CMEMS; http://marine.copernicus.eu/). Seven stations were sampled in E1 (Stations 2 (outbound leg) and 13–19 (inbound leg)), with Stations 13–15, and 19 located at the western and eastern edges of the eddy, respectively, as inferred from the ADCP data. Following the cruise, we identified two other anticyclonic features that were inadvertently sampled (at lower resolution than E1), E2 (8°E; Stations 3, 4, and 11) and E3 (3.4°E; Stations 5 and 9).

2.2. Physiochemical Sample and Data Collection and Analysis

2.2.1. Hydrography

A rosette equipped with Sea-Bird SBE 9/11 CTD and oxygen (Sea-Bird SBD 43) sensors and 24 12-L Niskin bottles was deployed at each of the 24 SAMBA stations. Direct salinity measurements made using a Portasal 8410A salinometer calibrated with IAPSO seawater standards (OSIL) verified the accuracy of the conductivity sensor, while the oxygen sensor was calibrated against discrete measurements of dissolved oxygen concentrations made by Winkler titration (Carpenter, 1965; Grasshoff et al., 1983). The mixed-layer depth (MLD) was determined from profiles of potential density anomaly (σ_θ; calculated from measured temperature, salinity, and

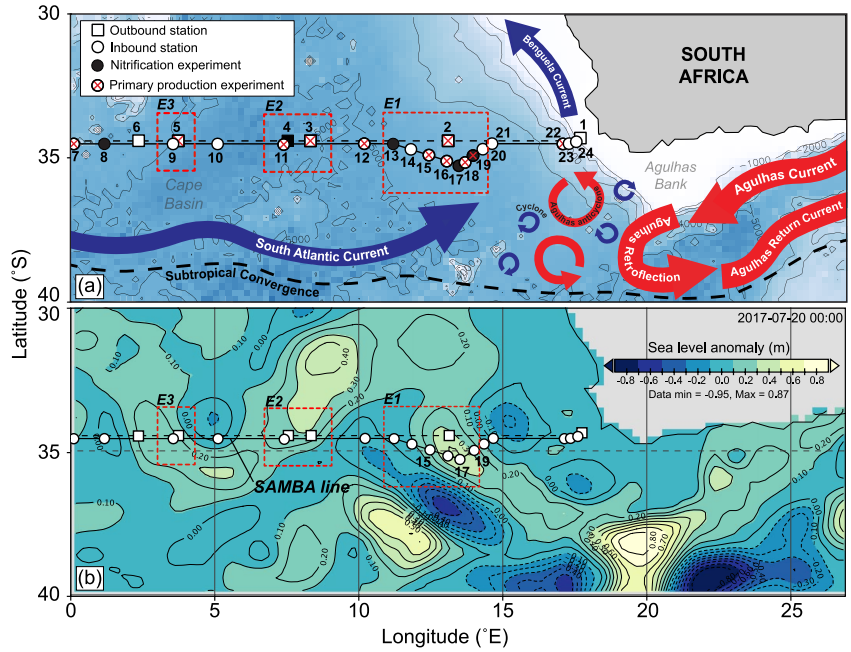

Figure 1. (a) Map showing the cruise track along the South Atlantic MOC Basin-wide Array line, overlaid on the regional bathymetry GEBCO 2021 Grid (https://doi.org/10.5285/c6612cbe-50b3-0cff-e053-6c86abc09f8f), for the outbound (dashed line, square station markers) and inbound (solid line, circle stations markers) legs of the cruise, with conductivity-temperature-depth stations indicated by the markers and numbers. Red crosses show the primary production stations and filled circles indicate the nitrification stations. The dashed red boxes enclose stations located within Agulhas eddies; these are labeled E1 (eddy 1), E2 (eddy 2), and E3 (eddy 3). The colored arrows represent the approximate positions of the relatively warm (red) and cool (blue) currents that dominate the surface flow around South Africa. Also shown is the approximate position of the Subtropical Convergence, which divides the South Atlantic from the Southern Ocean. (b) Map showing the cruise track and sampling stations overlaid on the sea level anomaly (SLA; in m) plotted for the 20 July 2017. Solid contours and green/yellow colors show positive SLAs while dashed contours and dark blue colors show negative SLAs. The SLA data were obtained from ¼ horizontal resolution daily near-real-time satellite data acquired from the multi-mission Level 4 satellite gridded product SEALEVEL_GLO_PHY_L4_NRT_OBSERVATIONS_008_046.

pressure) using the criterion of $\Delta\sigma_\theta = 0.03$ kg m^{-3} relative to σ_θ at 10 m (de Boyer Montégut et al., 2004). The depth of the euphotic zone (z_{eu}) was taken to be the penetration depth of 0.1% of surface photosynthetically active radiation (PAR), measured using a Seabird PAR sensor integrated with the CTD platform. While no CTD data are available for Station 6, nutrient and chlorophyll samples were collected at this station.

2.2.2. Nutrient Concentrations

Seawater samples were collected throughout the water column following GO-SHIP protocols (Hydes et al., 2010) in duplicate 50 mL polypropylene tubes for NO_3^-, silicic acid ($Si(OH)_4$), and NO_2^-, and in duplicate 50 mL high-density polyethylene (HDPE) bottles that had been "aged" with orthophthaldialdehyde working reagent (OPA-WR) for NH_4^+ (Smith et al., 2022). Nutrient samples were stored in the dark at 4°C until analysis, which occurred shipboard within 24 hr of collection. NH_4^+ samples from Stations 1–11 were measured shipboard, while the remainder (select profiles collected between Stations 12–22) were frozen and analyzed ashore following the cruise. There was no difference between samples measured at sea versus ashore.

The concentrations of NO_3^- and $Si(OH)_4$ were measured using a Lachat QuickChem® flow injection auto-analysis (FIA) platform in a configuration with a detection limit of 0.12 µmol L^{-1} for NO_3^- and 0.10 µmol L^{-1} for $Si(OH)_4$ (Egan, 2008; Wolters et al., 2002). Standards of varying concentrations were run after every 10 samples to monitor instrument performance and enable drift correction. The NO_2^- concentrations were analyzed manually using benchtop colorimetric methods (Strickland & Parsons, 1972), with absorbance measured using a Thermo Scientific Genesis 30 Visible spectrophotometer (detection limit of 0.03 µmol L^{-1}). Aliquots of a certified reference material (JAMSTEC) were analyzed at the beginning and end of all FIA and manual runs to ensure measurement accuracy. The precision of the NO_3^-, $Si(OH)_4$, and NO_2^- measurements was ±0.2, ±0.2, and ±0.05 µmol L^{-1},

respectively. The NH_4^+ concentrations were measured fluorometrically by reaction with OPA-WR (Holmes et al., 1999) using a Turner Designs Trilogy fluorometer equipped with a UV module. Precision was ±0.01 μmol L^{-1} and the detection limit was 0.02 μmol L^{-1}.

2.2.3. Chlorophyll-a

Chlorophyll-a concentrations ([Chl-a]) were determined at six mixed-layer depths at all stations. From each depth, 500 mL aliquots of seawater were filtered through 25 mm-diameter 0.3 and 2.7 μm glass fiber filters (Sterlitech, GF-75 and Grade-D, respectively). The filters were immersed in 90% acetone in borosilicate test tubes and stored at −20°C for 24 hr to allow for chlorophyll-a extraction (Welschmeyer, 1994). Post-extraction, [Chl-a] was measured using a Turner Designs Trilogy fluorometer calibrated with an analytical standard (*Anacystis nidulans*; Sigma-Aldrich), with measured fluorescence corrected for the acetone and filter blank. [Chl-a] was computed for two phytoplankton size classes, pico- (0.3–2.7 μm) and (nano+micro) phytoplankton (hereafter, "$nano_+$phytoplankton"; >2.7 μm) as:

$$[\mathrm{Chl-a}]_{\mathrm{bulk}} = [\mathrm{Chl-a}]_{0.3\mu\mathrm{m}} \quad (1a)$$

$$[\mathrm{Chl-a}]_{\mathrm{pico}} = [\mathrm{Chl-a}]_{0.3\mu\mathrm{m}} - [\mathrm{Chl-a}]_{2.7\mu\mathrm{m}} \quad (1b)$$

$$[\mathrm{Chl-a}]_{\mathrm{nano+}} = [\mathrm{Chl-a}]_{2.7\mu\mathrm{m}} \quad (1c)$$

Here, $[\text{Chl-a}]_{0.3\mu m}$ and $[\text{Chl-a}]_{2.7\mu m}$ are the chlorophyll-a concentrations measured for the 0.3 and 2.7 μm filter collections from the same station and depth. $[\text{Chl-a}]_{0.3}$ is also the total chlorophyll-a concentration (i.e., "$[\text{Chl-a}]_{bulk}$").

2.2.4. NPP and N Uptake Experiments

NPP and N (as NO_3^- and NH_4^+) uptake experiments were conducted at 11 stations: Stations 2, 3, 5, 7 (outbound leg) and 11, 12, 15, 16, 18, 19, 22 (inbound leg), hereafter referred to as "primary production stations" (Figure 1a). Seawater was collected at approximately the same time every day from two (Stations 2–12) or three (Stations 15–22) euphotic zone depths at each station, corresponding to the penetration depths of 55% and 1% or 55%, 30%, and 1% of surface PAR, respectively. At each depth, seawater was pre-filtered through 200 μm mesh (to remove large grazers) into four 1-L clear polycarbonate bottles. Duplicate bottles were amended with either $^{15}NH_4Cl$ or $K^{15}NO_3$ (99 at-% tracer) to yield $^{15}NH_4^+$ and $^{15}NO_3^-$ enrichments of ∼10%; the ^{15}N enrichments were subsequently calculated using the measured NH_4^+ and NO_3^- concentrations. Additionally, $NaH^{13}CO_3$ (99 at-%) was added to the $^{15}NO_3^-$ bottles to yield a ^{13}C enrichment of ∼5%. Bottles were incubated in a custom-built deck-board incubator cooled with running surface seawater for 4–6 hr, with in situ light levels (55%, 30%, or 1% PAR) simulated using neutral-density screens. Experiments were terminated by filtration, with 500 mL seawater aliquots filtered through combusted (450°C for 8 hr) 0.3 μm GF-75 and 2.7 μm Grade-D filters. At Stations 2, 3, 5, 7, 11, and 12, additional polycarbonate bottles were amended and incubated as above, with 1 L aliquots filtered through 10 μm nylon mesh upon experiment termination. The particles on these filters ("microplankton") were resuspended in 30 mL of 0.2-μm filtered seawater, then re-filtered onto combusted GF-75s. All filters were stored in combusted foil envelopes at −80°C until analysis.

In the laboratory, filters were oven-dried at 40°C for 24 hr. Each filter was cored using a 20 mm punch to remove blank perimeter filter, with the core packaged into a tin capsule. To determine particulate organic carbon (POC) and nitrogen (PON) content and isotopic composition, pelletized filters were analyzed using a Flash 1112 elemental analyzer coupled to a Delta V Plus isotope ratio mass spectrometer (IRMS); the detection limits were 2 μg C and 1 μg N and the precision was ±0.005 at% for both C and N. Blanks (consisting of an unused cored and combusted filter + tin capsule) and laboratory running standards calibrated to international reference materials were run after every 5–10 samples. Daily standard curves (IRMS voltages against known C and N masses) were used to compute POC and PON content, with POC and PON concentrations ([POC] and [PON]) determined by normalizing to seawater volume filtered.

Rates of NPP and NO_3^- and NH_4^+ uptake (ρNO_3^- and ρNH_4^+) (nmol L^{-1} hr^{-1}) were calculated according to Dugdale and Wilkerson (1986), assuming an initial at% of 1.07% for C and 0.366% for N, by multiplying the specific carbon fixation (V_C) and N uptake rates (V_{NO3} and V_{NH4}) (hr^{-1}) by the coincident measured [POC] or [PON]. Daily rates were determined by multiplying the hourly rates by 10.5, the number of daylight hours experienced at 34.5°S in late July.

As with [Chl-a], biomass ([POC] and [PON]) and uptake rates were determined for two plankton size classes, pico- and nano$_+$plankton. At the stations where 10 μm filters were also collected, nano- (2.7–10 μm) and microplankton (10–200 μm) biomass and rates were determined separately:

$$X_{\text{nano}} = X_{2.7\mu\text{m}} - X_{10\mu\text{m}} \tag{2a}$$

$$X_{\text{micro}} = X_{10\mu\text{m}} \tag{2b}$$

Where X refers to either the biomass or the uptake rate measured for the 2.7 μm ($X_{2.7\mu\text{m}}$) or 10 μm ($X_{10\mu\text{m}}$) filter collections at the same station and depth.

2.2.5. NO_2^- Oxidation Rate Experiments and Laboratory Analyses

Measurements of NO_2^- oxidation are used here as a metric for nitrification as NO_2^- oxidation is the step in the nitrification pathway that produces NO_3^-. At five stations (Stations 4, 8, 13, 17, and 19; hereafter "nitrification stations"), NO_2^- oxidation experiments were conducted at eight depths (six within the upper 250 m, as well 500 and 1,000 m). At each depth, seawater was 200 μm-filtered into two 250 mL opaque HDPE bottles to which ^{15}N-NO_2^- tracer was added to yield a final $^{15}NO_2^-$ concentration of 0.1 μM. Immediately following tracer addition, a 30 mL T_{initial} subsample was collected from each bottle and frozen at −20°C. The remaining water was incubated for 24 hr, with samples from the upper 250 m placed in the deck-board incubators and those from 500 to 1,000 m in a 4°C cold room. At the end of the experiments, 30 mL T_{final} subsamples were collected and frozen.

In the laboratory, any NO_2^- remaining in the T_{initial} and T_{final} subsamples was removed via the addition of 5% (v/v) sulfamic acid (Granger & Sigman, 2009). Sample pH was then adjusted to ~7–8 using 2 M NaOH. The δ^{15}N (in permil (‰) versus N_2 in air, $= \{(^{15}N/^{14}N)_{\text{sample}}/(^{15}N/^{14}N)_{N2} - 1\} \times 1000$) of the sample NO_3^- was analyzed by the denitrifier method (Sigman, et al., 2001) using a Delta V Plus IRMS with custom-built purge-and-trap front end (Weigand et al., 2016).

The rate of NO_2^- oxidation ($NO_2^-{}_{\text{ox}}$; nmol L^{-1} d^{-1}) was calculated from the change in the concentration of $^{15}NO_3^-$ during the experiments, with any increase in [$^{15}NO_3^-$] between T_{initial} and T_{final} assumed to derive from $^{15}NO_2^-$ oxidation. $NO_2^-{}_{\text{ox}}$ was calculated as in Peng et al. (2015) as:

$$NO_{2\,\text{ox}}^- = \frac{\Delta[^{15}NO_3^-]}{f_{NO_2^-}^{15} \times T} \tag{3}$$

where $\Delta[^{15}NO_3^-]$ is the change in the $^{15}NO_3^-$ concentration between T_{initial} and T_{final}, computed from the δ^{15}N data; $f_{NO_2^-}^{15}$ is the fraction of the NO_2^- pool labeled with ^{15}N at the beginning of the experiment, calculated from the volume of ^{15}N tracer added and the measured ambient NO_2^- concentrations, and T is the length of the incubation (days). The detection limit, calculated as the NO_3^- production rate necessary to cause a 2‰ increase in the δ^{15}N of NO_3^- relative to the T_{initial} value (Santoro et al., 2013), ranged from 0.01 to 0.32 nmol L^{-1} d^{-1}.

The $^{15}NO_2^-$ tracer was added to the incubation bottles to yield a final concentration of 0.1 μmol L^{-1}, which is typical for nitrification experiments (Ward, 2011). However, given the low ambient NO_2^- concentrations characteristic of oligotrophic waters, this amendment may have enhanced the oxidation rates, particularly given the (limited) evidence for a half-saturation constant for NO_2^- oxidation (i.e., K_m; the concentration of NO_2^- at which the rate of NO_2^- oxidation is half the maximum achievable rate) of ≤0.25 μmol L^{-1} d^{-1} (Mdutyana et al., 2022; Olson, 1981; Sun et al., 2017). We thus calculated revised NO_2^- oxidation rates following Diaz and Raimbault (2000), Horak et al. (2013), and Rees et al. (1999) as:

$$NO_{2\,\text{revised}}^- = \frac{NO_{2\,\text{ox}}^-}{\frac{\left[NO_{2\,\text{amb}}^- + NO_{2\,\text{tracer}}^-\right]}{K_m + \left[NO_{2\,\text{amb}}^- + NO_{2\,\text{tracer}}^-\right]} \times \frac{K_m + \left[NO_{2\,\text{amb}}^-\right]}{\left[NO_{2\,\text{amb}}^-\right]}} \tag{4}$$

where $NO_2^-{}_{\text{revised}}$ (nmol L^{-1} d^{-1}) is the rate of NO_2^- oxidation "corrected" for potential stimulation due to $^{15}NO_2^-$ tracer addition, $NO_2^-{}_{\text{ox}}$ is the original NO_2^- oxidation rate (Equation 3), $NO_2^-{}_{\text{amb}}$ is the measured ambient NO_2^- concentration, $NO_2^-{}_{\text{tracer}}$ is the concentration of $^{15}NO_2^-$ added to the incubation bottles, and K_m is the half-saturation constant for NO_2^- oxidation. We use K_m = 95.5 nmol L^{-1}, which was derived empirically from NO_2^- oxidation kinetics experiments conducted during the cruise.

2.2.6. Water-Column Integration

At each primary production station, uptake rates were trapezoidally integrated over the euphotic zone. The rates were first integrated using data from the 1% and 55% PAR depths or, if available, the 1%, 30%, and 55% PAR depths, after which the integration was extended to the 0.1% PAR depth (i.e., z_{eu}) by assuming a rate of 0 μmol L^{-1} d^{-1} at z_{eu}. For the stations with rate measurements from three light depths, the euphotic zone-integrated rates are similar (2% ± 10% difference on average) to those calculated using data from two light depths only, validating our use of integrated values for stations at which we have data from two depths.

The *f*-ratio (shorthand for "flux ratio") at each station ($f\text{-ratio}_{measured}$) was calculated using the euphotic zone-integrated uptake rates following Eppley and Peterson (1979) as:

$$f-\text{ratio}_{\text{measured}}=\frac{\rho NO_3^-}{\rho NO_3^- + \rho NH_4^+} \quad (5)$$

For mixed-layer nitrification, we trapezoidally integrated $NO_2^-{}_{ox}$ between the surface (15 m) and the MLD. At stations without data from 15 m, the closest surface measurement was used. Where measurements were lacking at the MLD, rates were estimated by linearly interpolating between the nearest rate measurements above and below the MLD. For logistical reasons, the nitrification and N uptake experiments were not conducted at the same stations (except at Station 19; Figure 1a). Below, we make some calculations that require an estimate of the coincident rates of N uptake and nitrification (e.g., when correcting the *f*-ratio for in situ nitrification; see Section 4.6). Thus, NO_2^- oxidation rates measured at nearby stations and/or at stations characterized by similar hydrography were taken as representative of the nitrification rates at the N uptake stations. All uptake stations were paired with a nitrification station (Table S2 in Supporting Information S1) except for Station 22 in the Benguela upwelling region where nitrification was not measured; Station 22 is thus excluded from any analysis requiring coincident N uptake and nitrification rates.

To account for the effect of regenerated NO_3^- (produced in the mixed-layer by nitrification) on estimates of carbon export potential, we recalculated the *f*-ratio using the mixed-layer integrated N uptake and NO_2^- oxidation rates (Mdutyana et al., 2020; Peng et al., 2018) as:

$$f-\text{ratio}=\frac{\rho NO_3^- - NO_{2\text{revised}}^-}{\left(\rho NO_3^- + \rho NH_4^+\right)} \quad (6)$$

3. Results

3.1. Hydrography and Eddy Characterization

The stations sampled along the SAMBA transect spanned a broad zonal region characterized by a high degree of hydrodynamic variability (Figure 1b and Figure S2 in Supporting Information S1). Four stations (Stations 1 and 22–24) were located near the continental slope in the southern Benguela upwelling region, with the remainder (Stations 2–21) situated considerably further offshore. We refer to these two groups as "Coastal" and "Open Ocean" stations, respectively.

Using SLA (Figure 1b and Figure S1 in Supporting Information S1), CTD data (Figures 2, 3, and Figure S3 in Supporting Information S1), and ADCP data (Figure S2 in Supporting Information S1), we identified three relatively young (formed in December 2016; Figure S1 in Supporting Information S1) asymmetrical eddies along the transect; E1, E2, and E3 (Figure 1a). The centers of these features were characterized by a positive SLA of 0.42 m, 0.47 m, and 0.31 m, respectively. However, only E1 was sampled at a resolution that allowed its "true" center to be characterized using the CTD and discrete data. The SLA product clearly shows the asymmetry of E1, such that its western (leading) and eastern (trailing) edges might be expected to be hydrodynamically different; however, we note that E1 was sampled on an unequally horizontally spaced grid, which has been shown to yield a distorted view of eddy physical and chemical fields (Martin & Richards, 2001). Alongside the effects of the various submesoscale dynamics ongoing in the CB, sampling bias may contribute to, although is unlikely to fully account for, the apparent differences between the eastern edge of the eddy (Station 19; characterized by strong physical and chemical gradients) and its more diffuse western edge (Station 13, 14, and 15) (Figures 2 and 3).

At the Open Ocean stations, the MLD ranged from 52 to 282 m (average of 194 m), with the shallowest MLD at Station 19 at the eastern edge of E1 and the deepest at Station 3 in E2, followed by Station 17 in the center of

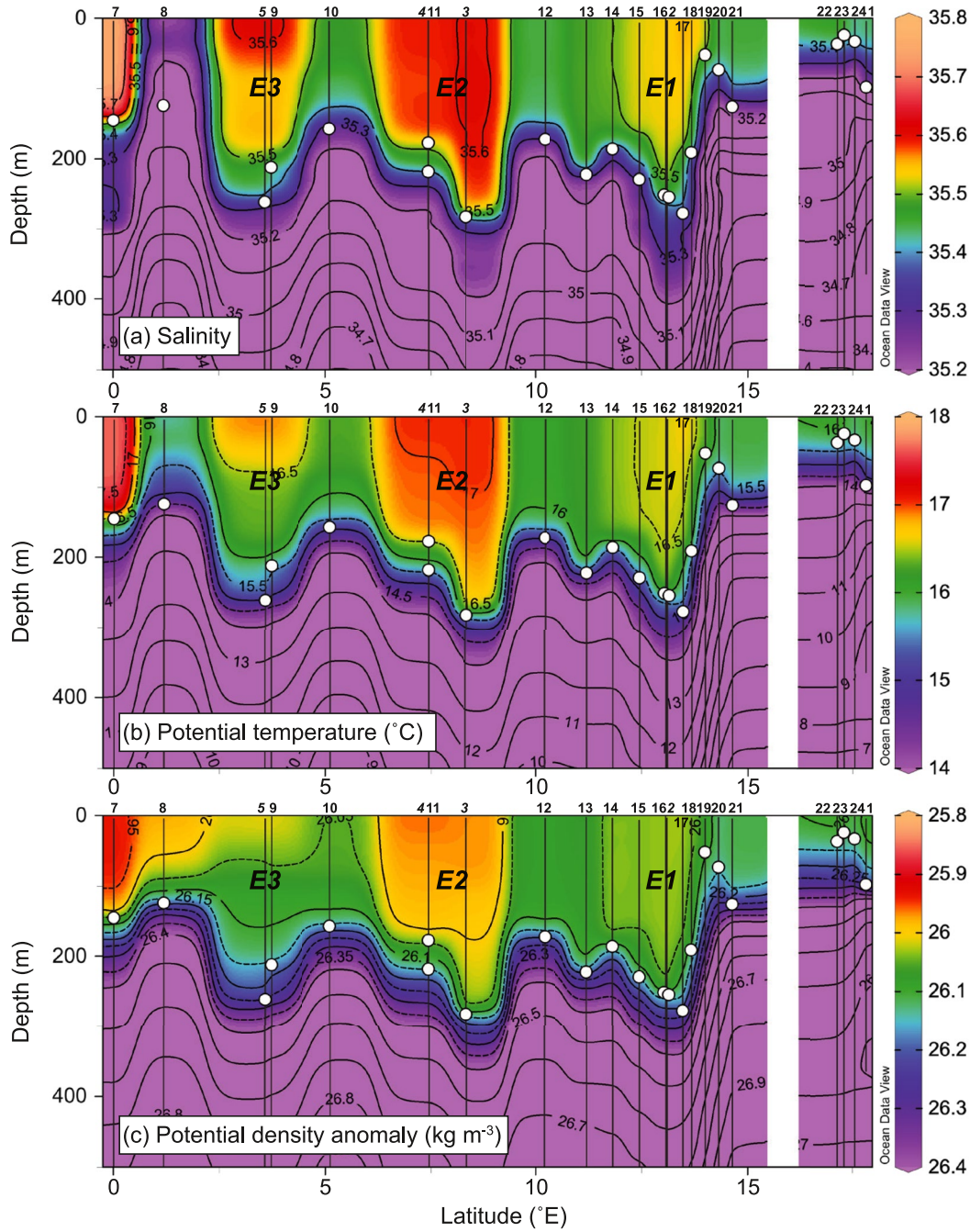

Figure 2. Section plots of (a) practical salinity, (b) potential temperature (°C), and (c) potential density anomaly (kg m^{-3}) over the upper 1,000 m of the combined outbound and inbound transect. On panel (a), eddy numbers are inscribed within each eddy (E1, E2, and E3), evident as high salinity features, and stations are numbered above the panels (outbound stations in italics (1–6), inbound stations in non-italics (7–24)). White circles indicate the mixed layer depth. Note the reversed color axis for panel (c).

E1 (277 m) (Figure 2; Table S1 in Supporting Information S1). The mixed layer was significantly deeper than z_{eu} at all but Stations 19 and 20 where the MLD and z_{eu} converged due to isopycnal shoaling at the eastern edge of E1. While similar isopycnal tilting was not observed at the western edge of E1 (Stations 13–15), the MLD was nonetheless shallower than in the center of the eddy (186–229 m vs. 277 m). Coastal Stations 22–24 were characterized by shallow MLDs (24–37 m) that were similar to z_{eu} (~45 m), while Station 1 had a MLD of 98 m and z_{eu} of 75 m.

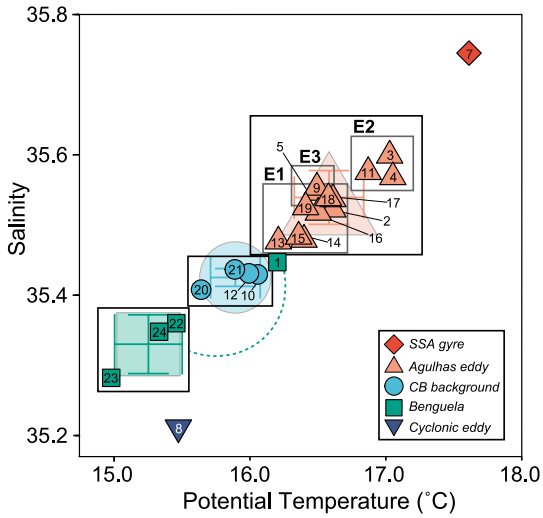

Figure 3. Average mixed-layer practical salinity versus potential temperature (°C) for individual stations (dark colors, small symbols) and hydrographic categories (light colors, large symbols). All conductivity-temperature-depth (CTD) stations sampled during the outbound and inbound cruise transects are included, except Station 6 for which there are no CTD data. Hydrographic category shapes are centered around the mean values, with error bars representing the category standard deviations. Stations located in the anticyclonic eddies are grouped within labeled gray boxes (E1, E2, and E3). The dashed green line indicates that Station 1, despite being located in the Benguela upwelling system, is characterized by significantly different hydrographic parameters from the other Benguela stations (see Text S1 in Supporting Information S1 for details). As such, this station is excluded from the Benguela category averages.

3.2. Station Categorization From Mixed-Layer Hydrography

Because of the hydrographic complexity of the CB, stations were grouped according to their physical characteristics rather than examined individually. We used average mixed-layer potential temperature and practical salinity measurements (Figure 3), along with depth profiles of salinity (Figure S2 in Supporting Information S1) and SLA data (Figure 1b), to assign each station to one of five groups: (a) *Benguela*, (b) *Cyclonic eddy*, (c) *CB background*, (d) *Agulhas eddy*, or (e) *Subtropical South Atlantic* (*SSA*) *gyre*. Station 6, for which we have no CTD data, was not assigned to a group. The *Benguela* group consists of all stations referred to above as Coastal, while the other groups encompass the stations characterized as Open Ocean. Because of the high volume of Agulhas leakage into the CB and the subsequent persistent vigorous mixing (Boebel et al., 2003), all our stations were likely affected by leakage to some extent, at least in the upper water column, resulting in subtle (but nonetheless clear) differences among them. We rely here on mixed layer properties in our station characterization because our focus is on shallow biogeochemical processes.

The mixed layer of the *SSA gyre* station (Station 7, furthest from shore) had the warmest (17.6°C) and most saline (35.7) waters of the transect (Figure 3 and Figure S2 in Supporting Information S1) and was associated with no SLA (Figure 1b). By contrast, the *Cyclonic eddy* station (Station 8) had a cooler (15.5°C) and less saline (35.2) mixed layer, likely due to upwelling of subsurface waters (Hall & Lutjeharms, 2010), which may also explain its shallower MLD (124 m) compared to the surrounding stations. Station 8 coincided with a weak negative SLA (−0.04 m), suggesting that the cyclonic eddy may have been a remnant of a once stronger feature. *Agulhas eddy* stations appeared as localized regions of warm (16.6 ± 0.3°C) and saline (35.5 ± 0.0) waters, constituting a mixture of Agulhas Current waters (Tropical and Subtropical Surface Waters, and Tropical and Subtropical Thermocline Waters), Subantarctic Surface Water, and South Atlantic Surface Water (Rigg, 1995). This group includes Stations 2–5, 9, 11, and 13–19. The mixed-layer properties most closely resembled Subtropical Surface Water ($T = 17.7$°C, $S = 35.6$; Bennett, 1988), albeit with lower average temperatures, likely because the regional negative heat flux reaches a maximum in winter (Walker & Mey, 1988), augmented by the influence of lateral mixing. Stations 1 and 22–24 were geographically located in the Coastal region of the transect (*Benguela* stations), yet Station 1 had a notably higher mixed-layer temperature (16.2°C) and salinity (35.5) than Stations 22–24 (15.3 ± 0.2°C, 35.3 ± 0.0), similar to the *Agulhas eddy* stations. A possible explanation is the passage of an Agulhas filament or other leakage feature (Lutjeharms & Cooper, 1996). This notion is consistent with the ADCP data that show a higher northward velocity at Station 1 at the time of sampling than was measured 10-days later when Stations 22–24 were occupied (Figure S2 in Supporting Information S1). Thus, while we characterize Station 1 as *Benguela* because of its geographic location, we exclude it from the *Benguela* category averages. As the CB is inundated with mesoscale and (related) submesoscale features, it is difficult to define a mean "background" hydrography that excludes the influence of Agulhas leakage. Here, we define the *CB background* stations (Stations 10, 12, 20, and 21) as those that were the least distinctive in terms of temperature, salinity, and SLA, and that appeared as a transition between *Agulhas eddy* and *Benguela* stations (Figure 3). The *CB background* group had an average mixed-layer temperature of 15.7 ± 0.6°C and salinity of 35.4 ± 0.1.

3.3. Nutrient and Biomass Distributions

Mixed-layer NO_3^- concentrations were fairly homogenous and generally decreased westward toward the SSA gyre (Figure 4a). Coastal stations were characterized by higher mixed-layer NO_3^- (3.9 ± 1.1 μmol L^{-1}) than Open Ocean stations (2.1 ± 0.9 μmol L^{-1}), as expected for shallow waters influenced by upwelling (Flynn et al., 2020). We observed a typical anticyclonic eddy-like nutrient distribution in the mixed-layer of E1, with lower average mixed-layer NO_3^- at the eddy center (Stations 2 and 16; 2.1 ± 0.0 μmol L^{-1}) than at its eastern (Station 19;

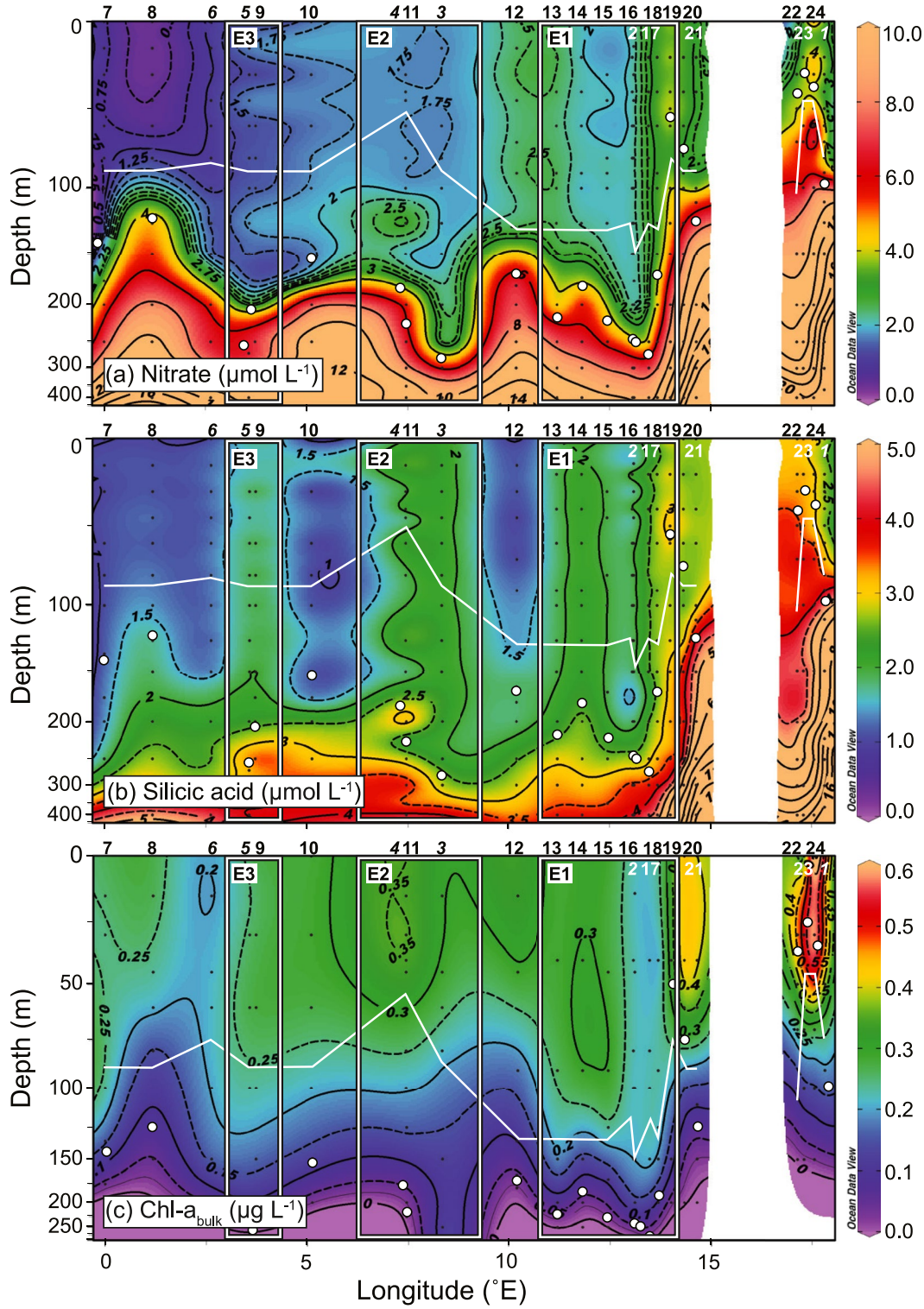

Figure 4. Section plots of (a) nitrate and (b) silicic acid concentrations (μmol L^{-1}) over the upper 400 m, and (c) bulk chlorophyll-a ($Chl\text{-}a_{bulk}$) concentrations (μg L^{-1}) over the upper 250 m of the combined outbound and inbound transect. The eddies are indicated by labeled white boxes (E1, E2, and E3) and the station numbers are included above each panel (outbound stations in italics (1–6), inbound stations in non-italics (7–24)). The horizontal white line indicates the depth of the euphotic zone, taken here to be the penetration depth of 0.1% of photosynthetically active radiation, and the white circles show the mixed layer depth.

4.0 μmol L^{-1}) and western (Station 13; 2.5 μmol L^{-1}) edges. The mixed-layer NO_3^- concentrations at the *CB background* stations ranged from 1.7 μmol L^{-1} at Station 10 to 2.5 μmol L^{-1} at Station 12, with the latter station (which was located adjacent to E1) possibly influenced by eddy mixing. An eddy-like nutrient pattern was not apparent in E2 and E3, presumably due to the low sampling resolution. In E3, Stations 5 and 9 were located very close together but sampled 2 days apart and the mixed-layer NO_3^- concentrations were 2.6 and 1.0 μmol L^{-1}, respectively, revealing the potential for small-scale intra-eddy variability on short timescales.

Generally, the zonal trends in $Si(OH)_4$ concentration differed from those of NO_3^-. Mixed-layer $Si(OH)_4$ was higher at the *Agulhas eddy* than the non-eddy Open Ocean stations (excluding Stations 20 and 21), with average concentrations of 2.2 ± 0.5 and 1.1 ± 0.1 μmol L^{-1}, respectively (Figure 4b). Interestingly, elevated $Si(OH)_4$ has been observed previously in an Agulhas eddy (surface concentrations of 3.0 ± 0.0 μmol L^{-1} in the eddy center, 2.2 ± 0.1 μmol L^{-1} at the eddy edge, and 1.6 ± 0.1 μmol L^{-1} outside the eddy in the Subtropical Convergence south of Africa (Dower & Lucas, 1993). Mixed-layer $Si(OH)_4$ concentrations were highest at the *Benguela* stations, averaging 3.2 ± 0.3 μmol L^{-1}.

Euphotic zone $[Chl\text{-}a]_{bulk}$ was fairly low across the transect, with surface values of 0.2–0.9 and 0.1–0.5 μg L^{-1} at the Coastal and Open Ocean stations, respectively (Figure 4c). $[Chl\text{-}a]_{bulk}$ was higher in the euphotic zone at the edges of E1 than at its center (reaching 0.5 vs. 0.2 μg L^{-1}), with $[Chl\text{-}a]_{bulk}$ in the eddy center appearing well-mixed over the upper 150 m. The Benguela $[Chl\text{-}a]_{bulk}$ was dominated by $nano_+$phytoplankton (77 ± 4% of $[Chl\text{-}a]_{bulk}$ on average), while at the Open Ocean stations, $nano_+$phytoplankton constituted 56% ± 8% of $[Chl\text{-}a]_{bulk}$ (Figure S4 in Supporting Information S1). The relative contribution of $nano_+$phytoplankton to $[Chl\text{-}a]_{bulk}$ generally declined westward, and was slightly higher at the edges of E1 than at its center.

Concentrations of POC and PON were only measured at the primary production stations and depths, resulting in limited vertical resolution. The euphotic-zone concentrations did not vary systematically across the transect, ranging from 2.3 to 7.8 μmol L^{-1} POC and 0.25–0.62 μmol L^{-1} PON (Figures 5a and 5b). On average, pico- and $nano_+$plankton contributed 25% ± 15% and 74% ± 12% of the POC and 32% ± 14% and 67% ± 12% of the PON, respectively. At the stations where nano- and microplankton were separated, pico-, nano-, and microplankton contributed 31% ± 11%, 46% ± 13%, and 22% ± 8% of the POC and 41% ± 12%, 43% ± 8%, and 16% ± 13% of the surface PON, respectively. Euphotic zone-integrated bulk POC:PON ratios averaged (9.3 ± 2.4):1, higher than the expected Redfield ratio of 6.63:1 (Figure 5c). The average picoplankton POC:PON ratio was (6.16 ± 1.3):1, while the $nano_+$plankton ratio was (10.3 ± 2.0):1. At the stations with separate nano- and microplankton measurements, the average POC:PON ratios were (9.7 ± 3.4):1 and (16.0 ± 8.6):1, respectively. The POC:PON ratios in excess of Redfield are likely the result of a significant contribution of carbon-rich detritus (Flynn et al., 2018; Van Oostende et al., 2017).

3.4. Primary Productivity and Nitrogen Uptake

NPP and N uptake experiments were conducted at stations in four hydrographic categories, the *SSA gyre* (Station 7), *CB background* (Station 12), *Benguela* (Station 22), and *Agulhas eddy* (Stations 2, 3, 5, 11, 15, 16, 18, and 19), with at least one station located in each of E1, E2, and E3. The microplankton size class was separated at six of the 11 primary productivity stations (Stations 2, 3, 5, 11, and 12). On average, the microplankton contribution to NPP, ρNO_3^-, and ρNH_4^+ was low, 2.1% ± 2.9%, 1.2% ± 1.4%, and 0.4% ± 0.4%, respectively, such that the rates associated with the $nano_+$plankton size class (i.e., 2.7–200 μm) at the stations without microplankton measurements can be taken as representative of nanoplankton (2.7–10 μm) activity.

Stations 2, 15, 16, 18, and 19 were located within E1. Here, surface NPP_{bulk} was higher at the eddy-edges than at its center (Figure 6a); NPP_{bulk} at edge Stations 15 and 19 was 754 ± 80 and 765 ± 41 nmol L^{-1} d^{-1}, respectively, whereas at the center Stations 16 and 2, NPP_{bulk} was 295 ± 1 and 348 ± 27 nmol L^{-1} d^{-1}. Station 18, located between an edge and center station, was characterized by an intermediate rate of 508 ± 160 nmol L^{-1} d^{-1}. Surface $\rho NO_3^-{}_{bulk}$ showed a similar pattern, with eddy-edge stations characterized by NO_3^- uptake rates of 48 ± 6 nmol L^{-1} d^{-1} (Station 15) and 73 ± 7 nmol L^{-1} d^{-1} (Station 19), and center stations by rates of 29 ± 10 nmol L^{-1} d^{-1} (Station 16) and 16 ± 4 nmol L^{-1} d^{-1} (Station 2) (Figure 6b). At the depth of 1% PAR, NPP_{bulk} in the center of E1 was 605 ± 81 nmol L^{-1} d^{-1} (Station 2) and 145 ± 10 nmol L^{-1} d^{-1} (Station 16), while edge-Station 15 hosted the highest rate of NPP_{bulk}, 742 ± 156 nmol L^{-1} d^{-1}. The trend in $\rho NO_3^-{}_{bulk}$ at 1% PAR was similar to the surface pattern, with higher rates at the eddy edges (32.9 ± 5.8–43.2 ± 16.7 nmol L^{-1} d^{-1}) and lower rates at the center

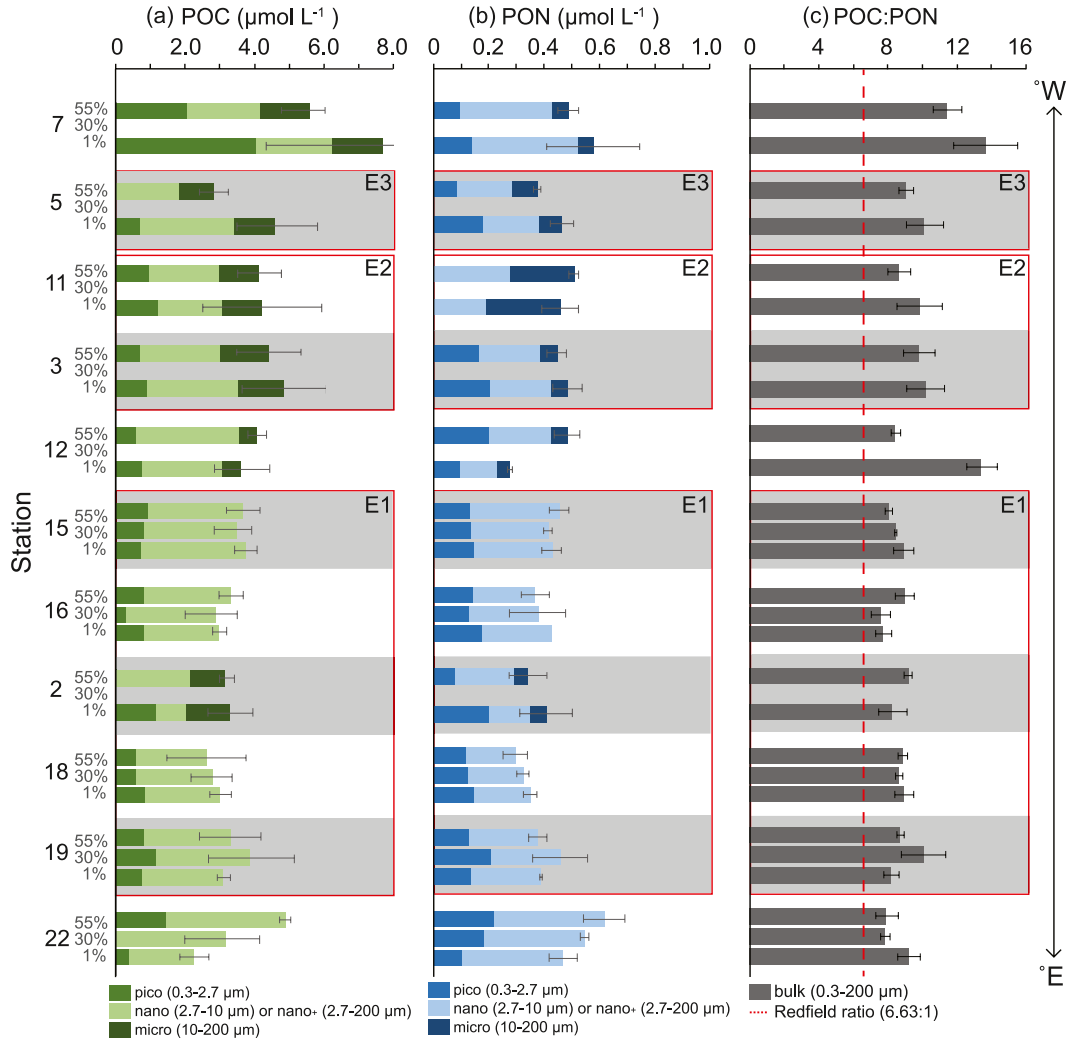

Figure 5. Size-fractionated concentrations (µmol L^{-1}) of particulate organic (a) carbon (particulate organic carbon [POC]) and (b) nitrogen (particulate organic nitrogen [PON]), along with (c) the bulk POC:PON ratio measured at various light levels at the primary production stations (top to bottom = west (open ocean) to east (coastal) along the transect). Red boxes denote the eddy stations and the red dashed vertical line on panel (c) indicates the Redfield ratio. Microplankton (i.e., >10 µm) data are only available for Stations 2–12; here, the nanoplankton size class ("nano−") refers to particles of 2.7–10 µm while at the other stations, the "$nano_+$" size fraction is shown (i.e., all particles >2.7 µm; see Text S1 in Supporting Information S1 for details). Data from the 30% photosynthetically active radiation depth are not available for Stations 2, 3, 5, 7, 11, and 12. The error bars shown on panels (a and b) (±1 standard deviation; $n = 2$) are for the bulk (i.e., >0.3 µm) measurements, while on panel (c), error was propagated according to standard statistical practices.

(8.7 ± 0.2–22.3 ± 1.2 nmol L^{-1} d^{-1}). By contrast, $\rho NH_4^+{}_{bulk}$ varied little between stations and depths within E1, except at Station 15 where the rate at all depths was double that of other E1 stations (Figure 6c). Across E1, $\rho NH_4^+{}_{bulk}$ was on average 48% ± 28% lower than $\rho NO_3^-{}_{bulk}$.

E2 and E3 were represented by Stations 3 and 11 (E2) and Station 5 (E3), respectively. In general, NPP and N uptake were lower at the E2 and E3 stations than at the edges of E1, and similar to or slightly higher than those measured at the center of E1. Additionally, $\rho NO_3^-{}_{bulk}$ and $\rho NH_4^+{}_{bulk}$ were similar in E2 while in E3, $\rho NO_3^-{}_{bulk}$ was higher (although with high uncertainty) (Figure 6).

Three primary productivity experiments were conducted outside the eddies, at Stations 7 (*SSA gyre*), 12 (*CB background*), and 22 (*Benguela*). At Station 7, NPP_{bulk}, $\rho NO_3^-{}_{bulk}$, and $\rho NH_4^+{}_{bulk}$ were higher at 1% PAR than at the surface, and $\rho NO_3^-{}_{bulk}$ was similar to $\rho NH_4^+{}_{bulk}$ (Figure 6). High surface rates of NPP_{bulk} were measured at Stations 12 (767 ± 35 nmol L^{-1} d^{-1}) and 22 (801 ± 248 nmol L^{-1} d^{-1}), with considerably lower rates at 1%

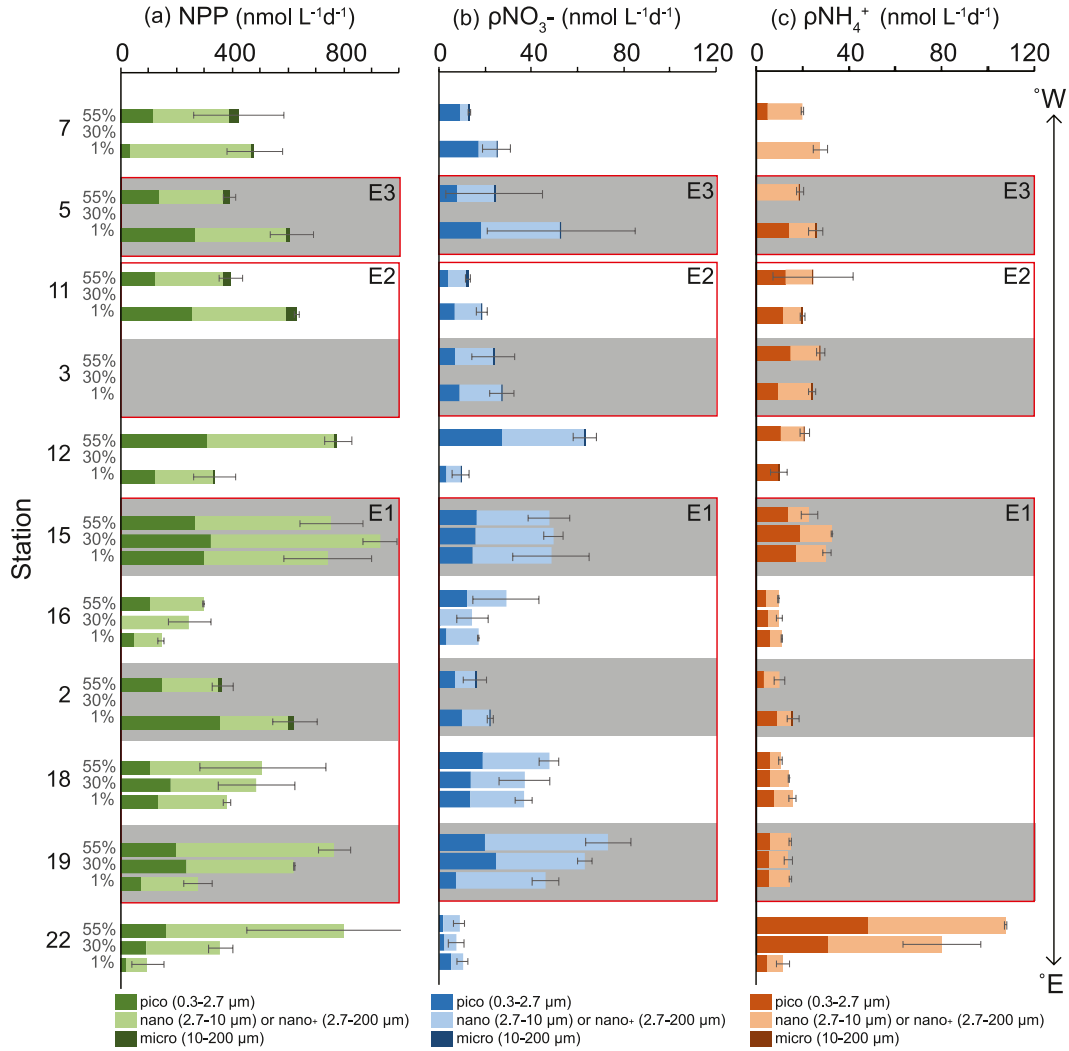

Figure 6. Size-fractionated rates (nmol L^{-1} d^{-1}) of (a) net primary production (NPP), (b) nitrate uptake (ρNO_3^-), and (c) ammonium uptake (ρNH_4^+) measured at various light levels at the primary production stations (top to bottom = west (open ocean) to east (coastal) along the transect). Red boxes indicate the eddy stations. Microplankton (i.e., >10 µm) data are only available for Stations 2–12; here, the nanoplankton size class ("nano−") indicates particles of 2.7–10 µm while at the other stations, the "$nano_+$" size fraction is shown (i.e., all particles >2.7 µm; see Text S1 in Supporting Information S1 for details). NPP was not measured at Station 3, and data from the 30% photosynthetically active radiation depth are not available for Stations 2, 3, 5, 7, 11, and 12. The error bars (±1 standard deviation; $n = 2$) are for the bulk (i.e., >0.3 µm) measurements (i.e., the sum of pico-, nano- (or $nano_+$), and microplankton).

PAR (330 ± 3 and 98 ± 40 nmol L^{-1} d^{-1}, respectively). $\rho NO_3^-{}_{bulk}$ and $\rho NH_4^+{}_{bulk}$ followed the same trend at Station 12, with higher rates at the surface (63.3 ± 5 and 20.8 ± 2.3 nmol L^{-1} d^{-1}) than at 1% PAR (9.5 ± 3.8 and 9.6 ± 3.5 nmol L^{-1} d^{-1}). By contrast, NPP at Station 22 was primarily supported by NH_4^+, the uptake rate of which reached a transect maximum at this station (107.9 nmol L^{-1} d^{-1}). $\rho NO_3^-{}_{bulk}$ was low throughout the euphotic zone at Station 22, averaging 8.7 ± 1.0 nmol L^{-1} d^{-1}.

Some of the trends observed for NPP_{bulk}, $\rho NO_3^-{}_{bulk}$, and $\rho NH_4^+{}_{bulk}$ in Figure 6 are eroded once the rates are integrated to 0.1% PAR (Figure 7a). This change occurs because many of the stations where high depth-specific uptake rates were measured were characterized by comparatively shallow euphotic zones, while those that hosted lower rates had deeper euphotic zones (e.g., compare Station 19 where z_{eu} = 75 m to Station 2 where z_{eu} = 150 m). As a result, the eddy edge versus center difference is weakened, although maximum rates of NPP_{bulk} and $\rho NO_3^-{}_{bulk}$ are still observed at an edge-station (Station 15; 93.3 mmol C m^{-2} d^{-1} and 5.2 mmol N m^{-2} d^{-1}) and some of the lowest rates occur in the center of E1 (Station 16; 21.1 mmol C m^{-2} d^{-1} and 1.5 mmol

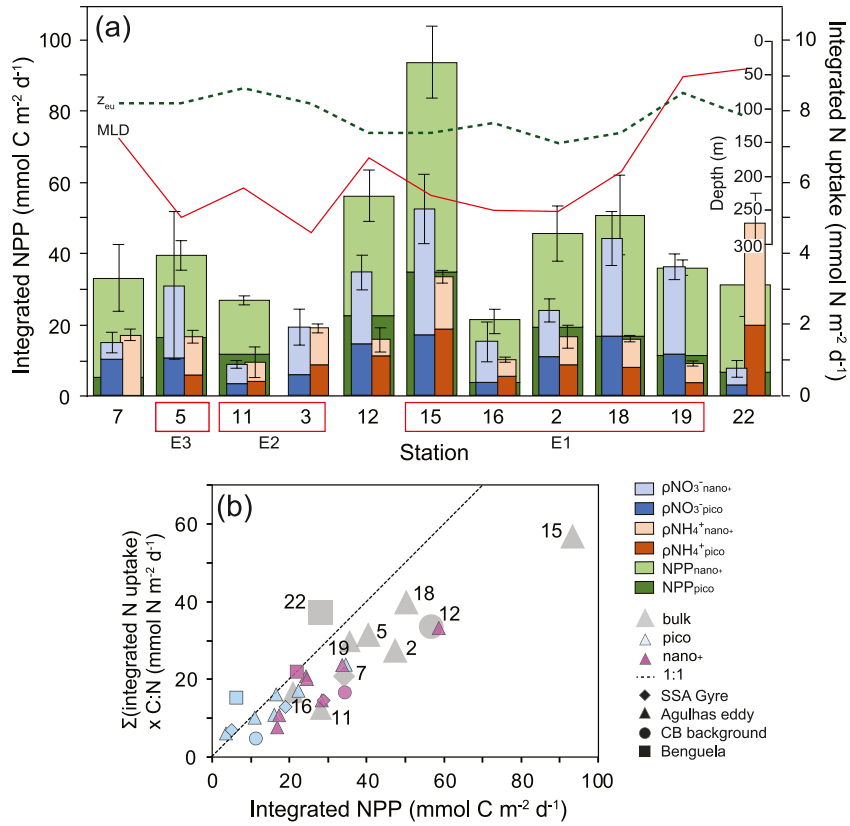

Figure 7. (a) Euphotic zone-integrated size-fractionated rates (mmol m^{-2} d^{-1}) of net primary production (NPP) and nitrate (ρNO_3^-) and ammonium uptake (ρNH_4^+) at the primary production stations along the combined outbound and inbound transect. The pico- and $nano_+$ rates are shown as stacked bars, with their sum yielding the bulk integrated rate at each station. Separate microplankton rates are not shown as the values were extremely low (see Text S1 in Supporting Information S1 for details). Note the separate *y*-axes for NPP (left) and N uptake (right). Eddy stations are indicated on the *x*-axis by the red boxes, and the mixed-layer and euphotic zone depths are shown by the solid and dashed lines, respectively. (b) Euphotic zone-integrated rates (bulk, pico, and $nano_+$) of NPP versus total nitrogen uptake (i.e., ($\rho NO_3^- + \rho NH_4^+$) × the Redfield C:N ratio of 106:16). The dashed diagonal line represents the 1:1 relationship expected if the rate of NPP were entirely supported by the measured rate of NO_3^- plus NH_4^+ uptake.

N m^{-2} d^{-1}). Across the transect, $nano_+$plankton contributed more to integrated NPP_{bulk}, $\rho NO_3^-{}_{bulk}$, and $\rho NH_4^+{}_{bulk}$ (66% ± 11%, 61% ± 12%, and 56% ± 19%, respectively) than picoplankton.

Except at Station 22, integrated bulk and size-fractionated NPP and total N uptake normalized to the Redfield ratio (i.e., ($\rho NO_3^- + \rho NH_4^+$) × 106:16) resulted in data points falling below the 1:1 slope in Figure 7b. The implication is that some fraction of the NPP was supported by an N source that we did not measure. Alternately, phytoplankton could be fixing carbon and consuming N in a ratio >>6.63:1. Such carbon overconsumption has been shown to occur when phytoplankton experience extreme nutrient limitation (Obernosterer & Herndl, 1995); however, since mixed-layer NO_3^- was relatively elevated across our transect, highly non-Redfieldian phytoplankton growth is unlikely. In contrast to the other stations, both pico- and $nano_+$plankton at Station 22 fixed less carbon than the stoichiometric quantity expected from total N uptake (i.e., resulting in the data points falling above the 1:1 slope in Figure 7b), possibly because a high ambient NH_4^+ supply, typical of coastal waters (Harrison, 1978), allowed for NH_4^+ uptake by both auto- and heterotrophic plankton, with the latter group fixing no carbon (Mdutyana et al., 2020).

3.5. NO_2^- Oxidation Rates

NO_2^- oxidation was measured at five stations, four of which were *Agulhas eddy* stations (Stations 4 (E2), 13 (E1 western edge), 17 (E1 center), and 19 (E1 eastern edge)), with the fifth characterized as a *Cyclonic eddy* station

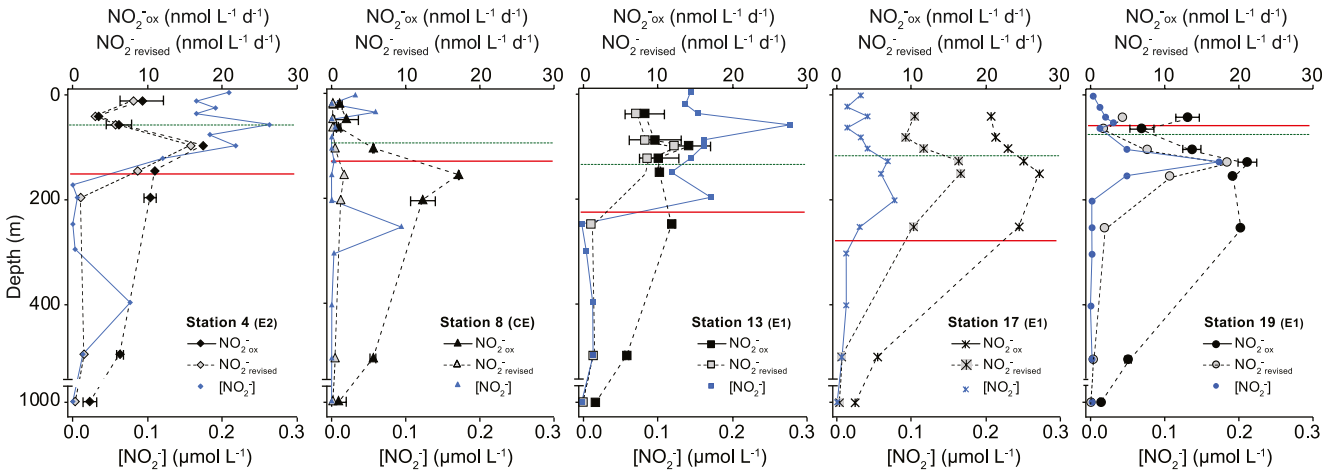

Figure 8. Depth profiles of nitrite (NO_2^-) oxidation rates ($NO_2^-{}_{ox}$; nmol L^{-1} d^{-1}; top *x*-axis), revised NO_2^- oxidation rates ($NO_2^-{}_{revised}$; nmol L^{-1} d^{-1}; top *x*-axis), and NO_2^- concentrations (μmol L^{-1}; bottom *x*-axis) at the nitrification stations. The dashed lines between the nitrification rate data are intended to guide the eye, and should not be taken to suggest interpolation with depth. The solid red and dashed green horizontal lines show the depth of the mixed layer and euphotic zone, respectively.

(Station 8). $NO_2^-{}_{revised}$ was elevated throughout the water column at the *Agulhas eddy* stations, but at or below detection at Station 8 (Figure 8). At all *Agulhas eddy* stations, the maximum $NO_2^-{}_{revised}$ rate occurred between 100 and 150 m (12.4–18.5 nmol L^{-1} d^{-1}), coincident with a high NO_2^- concentration. At Stations 4, 13, and 17, the maximum $NO_2^-{}_{revised}$ rate was observed near z_{eu} and within the mixed layer, whereas at Station 19, it was observed 50 and 75 m below z_{eu} and the mixed layer, respectively. The mixed layer-integrated $NO_2^-{}_{revised}$ rate was below detection at Station 8 and ranged from 0.16 to 3.33 mmol m^{-2} d^{-1} at the *Agulhas eddy* stations, with the highest rate computed for Station 17 and the lowest for Station 19, despite the latter hosting the highest depth-specific $NO_2^-{}_{revised}$ of 18.5 nmol L^{-1} d^{-1} at 125 m.

4. Discussion

The central goal of this study was to evaluate the effect of Agulhas leakage on phytoplankton productivity and nitrification in the CB by directly measuring these processes along a transect that intersected "background" Atlantic conditions and Agulhas leakage. Of the three eddies encountered during the cruise, E1 provided an opportunity to additionally investigate intra-eddy dynamics as this feature was sampled at high resolution—our discussion is thus largely focused on the E1 findings. Below, we first evaluate the influence of Agulhas eddies on NPP and NO_3^- and NH_4^+ uptake in the CB and discuss the potential drivers thereof. We then estimate carbon export potential across the transect, considering several complications associated with using NO_3^- uptake as a proxy for export production.

4.1. Phytoplankton Productivity in the Cape Basin and Agulhas Eddies

Eddy productivity and biomass distributions are broadly influenced by three types of processes (for a review, see McGillicuddy, 2016): (1) those that advect nutrients and phytoplankton horizontally via trapping (D'Ovidio et al., 2013; Flierl, 1981; Provenzale, 1999) and stirring (Martin, 2003); (2) those that affect the vertical velocity field and nutrient supply via processes such as eddy pumping (Falkowski et al., 1991) and eddy-wind interactions (Flierl & McGillicuddy, 2002; Stern, 1965); and (3) those that control phytoplankton exposure to light through their effect(s) on the MLD (linked to process (2)). Eddy trapping and stirring are common in regions such as the CB where nonlinear eddies import waters from elsewhere and stir the horizontal field through frequent eddy-eddy and eddy-front interactions. Indeed, stirring is hypothesized to be the dominant mesoscale mechanism by which eddies influence chlorophyll concentrations in the mid-latitudes (at timescales of weeks to months; Chelton et al., 2011). However, we focus here on processes (2) and (3) as our data set provides insights into the vertical tracer distributions in an Agulhas eddy, which is lacking in satellite-based studies of eddy productivity. Moreover, given the "snapshot" nature of our study, processes (2) and (3) are more relevant since they operate on shorter timescales than advective processes (Mahadevan, 2016). That said, the elevated mixed-layer $Si(OH)_4$

concentrations at the *Agulhas eddy* stations (Figure 4b) evince trapping and advection of biogeochemical properties originating in the Indian Ocean, with implications for plankton transport that warrant further investigation.

Across the transect, the z_{eu} and MLD varied considerably (Figures 2 and 4; Table S1 in Supporting Information S1). When the depths of these two layers are similar, phytoplankton are light-replete as they spend minimal time in the dark waters below the euphotic zone. Assuming non-limiting mixed-layer nutrient concentrations, this condition should yield elevated rates of productivity. By contrast, when the mixed layer is considerably deeper than the euphotic zone, phytoplankton are regularly mixed down into aphotic waters, which reduces photosynthesis and decreases the potential for carbon accumulation and export (Denman & Gargett, 1983; Holligan et al., 1984). Thus, eddy-related alterations to the MLD will have implications for productivity. Across the Open Ocean sector of our transect, except at Station 8, mixed-layer NO_3^- concentrations were non-zero (Figure 4), suggesting that NO_3^- availability was not the primary limitation on productivity. Since the mixed layer was nearly always deeper than z_{eu}, in many cases by >100 m, we propose that light availability was the major limiting factor for phytoplankton. We thus expected, and indeed observed, low rates of productivity in the center of E1 (Stations 2 and 16) where the MLD far exceeded the z_{eu}, and higher rates at the eddy edges (Stations 15 and 19) where the MLD shoaled toward z_{eu} (Figure 6). At the eastern edge of the eddy (Station 19), strong isopycnal shoaling raised the mixed layer above z_{eu}, releasing phytoplankton from light limitation and injecting nutrients into surface waters (Figures 4a and 4b; McGillicuddy et al., 1995). Such isopycnal shoaling can result from a variety of eddy-eddy, eddy-wind, and/or eddy-front interactions and is known to yield significant rates of upwelling that can increase eddy productivity (Mahadevan et al., 2008; Martin & Richards, 2001; Yoshimori & Kishi, 1994).

Our surface (55% PAR) measurements of [Chl-a], NPP, and NO_3^- uptake, and to a lesser extent, NH_4^+ uptake, were all higher at the edges of E1 than at its center (Figures 4c and 6, and Figure S5 in Supporting Information S1) where we suggest that light limitation impeded phytoplankton growth. Curiously, the mixed layer at Station 15 at the western edge of E1 was much deeper than z_{eu} (229 vs. 135 m), yet the surface rate of NPP was similar to that measured at Station 19 at the eastern eddy-edge where the mixed layer and euphotic zone were equivalently shallow. That NPP was elevated at Station 15 despite the decoupling of the MLD and z_{eu} may indicate a very recent deepening of the mixed layer.

Numerical models have shown that shoaling of anticyclonic eddy edges coupled with vertical mixing elevate biological productivity relative to the surrounding waters (Lima et al., 2002; Lovecchio et al., 2022; Mahadevan et al., 2008). Similarly, an increase in productivity has been directly observed for warm-core anticyclonic rings encountered near the Subtropical Convergence south of the Agulhas Retroflection (in this case originating from the Agulhas Current rather than the Retroflection; Dower & Lucas, 1993) and associated with the Gulf Stream (e.g., Gordon et al., 1982; Nelson et al., 1985; Olson & Evans, 1986), as well as in the Bering Sea (Mizobata et al., 2002), Tasman Sea (Scott, 1981), and North China Sea (Wang et al., 2018). In our study, however, the surface NPP and NO_3^- uptake rates at Station 12 (*CB background*) were as high as those measured at the eddy edges, as was the case for NPP at Station 22 in the *Benguela*. These observations raise the question of whether anticyclonic Agulhas eddies increase productivity at their edges, or only decrease it at their centers.

Here, we argue that Agulhas eddies enhance total and new production at their edges above background conditions. Integrating our rate data over the euphotic zone revealed different trends from those implied by the surface rates alone (Figure 7a). For instance, at Stations 12 and 22, NPP decreased between the surface and z_{eu}, by 57% and 88%, respectively (Figure 6a), which implies that the phytoplankton community was vertically stratified, likely due to weaker mixing at these non-eddy stations. By contrast, at many *Agulhas eddy* stations, the rates decreased far less with depth, suggesting strong vertical mixing of phytoplankton throughout the upper water column (e.g., at Station 15 in E1, NPP decreased by only 2% between the surface and z_{eu}, with the maximum rate measured at 30% PAR). The integrated rates of NPP and N uptake thus provide a more complete picture of phytoplankton productivity than the surface measurements alone. One implication of this observation is that productivity metrics based on surface proxies (e.g., satellite-derived chlorophyll-a concentrations) may underestimate the fertility of anticyclonic eddies.

The highest euphotic zone-integrated rate of NPP and N uptake occurred at the western edge of E1 (Station 15; Figure 7a). By contrast, the integrated rates at Station 19 at the eastern edge were relatively low, a result of its shallow z_{eu}. Nevertheless, it is likely that NO_3^- supplied vertically at the eastern edge of the eddy was entrained into E1, increasing euphotic zone NO_3^- concentrations and productivity at Station 18 (Figures 4a, 6a, and 7a). Low integrated rates of NPP and N uptake were observed at Station 16, which we consider most representative

of the eddy-center as it was sampled on the inbound leg of the cruise coincident with the other E1 stations (in contrast to Station 2, which, while categorized as eddy-center, was sampled almost a week prior to the other E1 stations). In comparison to Stations 15 (edge) and 16 (center), *CB background* Station 12 supported intermediate integrated rates of NPP and N uptake. Dower and Lucas (1993) observed a similar pattern in NPP associated with an Agulhas eddy encountered in the Subtropical Convergence south of South Africa. Mean integrated NPP (over the upper 100 m) was lowest in the eddy (23.9 ± 2.0 mmol C m^{-2} d^{-1}) and highest at its edges (37.7 ± 4.7 mmol C m^{-2} d^{-1}), with intermediate rates observed outside the eddy (33.6 ± 6.5 mmol C m^{-2} d^{-1}). In our study, the lowest rate of integrated NPP (measured at Station 16) was 21.1 ± 3.5 mmol C m^{-2} d^{-1}, while the highest (determined at Station 15) was 93.3 ± 10.1 mmol C m^{-2} d^{-1}. Outside the eddy at Station 12, we measured a rate of 56.7 ± 7.3 mmol C m^{-2} d^{-1}. Collectively, these studies suggest that Agulhas eddies enhance productivity at their edges and weaken it at their centers.

While strong trends were observed for NPP across the transect, the chlorophyll-a concentrations were fairly low and more patchy (Figure 4c; noting that patchiness is expected for regions of high (sub)mesoscale activity (Harris, 1980; Martin, 2003; Martin & Richards, 2001)). In general, the horizontal and vertical gradients in total chlorophyll-a were weak and appear to have been most strongly influenced by mixing, although we do observe elevated chlorophyll-a concentrations near the eastern edge of E1 and lower values at its center. The relative contribution of pico- versus $nano_{+}$phytoplankton to total chlorophyll-a increased from east to west, with E2 and E3 characterized by a higher ratio of pico- to $nano_{+}$phytoplankton than E1, similar to that measured at the *CB background* stations (Figure S3 in Supporting Information S1). The chlorophyll-a concentrations thus appear to record no eddy-related trends in phytoplankton size structure. This may be because eddy biology becomes progressively similar to the surrounding waters as eddies age and lose their unique primary producer communities (Gould & Fryxell, 1988; Hitchcock et al., 1985; Ortner et al., 1984) and genetic distinction (Villar et al., 2015). Given the mismatch between our measured surface chlorophyll concentrations and the integrated trends in NPP (Figure S4 in Supporting Information S1), we caution against using surface chlorophyll as a proxy for primary productivity across the CB.

4.2. Carbon Export Potential Across the Cape Basin: Trends and Possible Complications

Within the new production paradigm framework where phytoplankton NO_3^- consumption is assumed to equal new and export production (Dugdale & Goering, 1967), our NO_3^- uptake data suggest that carbon export potential was enhanced at the edges of E1 (Stations 15, 18, and 19), and lower at the eddy-center and background stations (Stations 2 and 16, and 7 and 12, respectively) (Figure 7a). The fraction of NPP that is potentially exported is often estimated using the *f*-ratio, with higher *f*-ratios indicating a stronger biological pump (Eppley & Peterson, 1979). In our study, the values of $f\text{-ratio}_{measured,}$ which assumes that NO_3^- and NH_4^+ uptake equate to new and regenerated production, respectively (Equation 5), are higher than anticipated for an oligotrophic system (Figure 9, light blue background bars; Eppley and Peterson (1979)). The average $f\text{-ratio}_{measured}$ at the *Agulhas eddy* stations is 0.62 ± 0.11, with little evidence of a gradient between the eddy edges and its center, and the *CB background* and *SSA gyre* station values are 0.69 and 0.48, respectively. By contrast, at Station 22 where one might expect a high *f*-ratio given the generally productive nature of the Benguela upwelling system (Andrews & Hutchings, 1980) the $f\text{-ratio}_{measured}$ is 0.08. We attribute this low value to NH_4^+ inhibition of NO_3^- uptake, which has been observed previously in the southern Benguela in winter (Flynn et al., 2018), along with enhanced NH_4^+ uptake, both of which are consistent with the elevated rates of NH_4^+ uptake measured at Station 22 (Figure 6c).

Using the new production paradigm as originally defined (i.e., as above) to quantify carbon export potential requires that (a) the rate of regenerated NO_3^- production due to mixed-layer nitrification is low relative to the supply and consumption of NO_3^- from below; (b) there is little to no consumption in the mixed layer of N deriving from N_2 fixation or atmospheric N deposition; and (c) other regenerated N forms such as DON support negligible rates of primary production (Bronk et al., 1994; Dugdale & Goering, 1967; Yool et al., 2007). Below, we assess the validity of these assumptions in the CB and discuss the implications for carbon export potential and the *f*-ratio.

4.2.1. Mixed-Layer Nitrification

Nitrification has not previously been measured in the CB, nor within Agulhas eddies. Mixed-layer NO_2^- oxidation rates ranged from 0.1 to 21.2 nmol L^{-1} d^{-1}, consistent with existing mid- and low-latitude open ocean

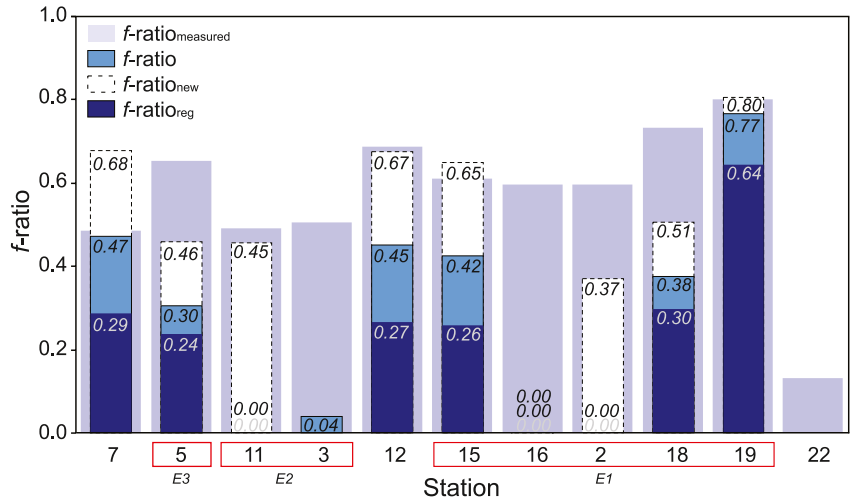

Figure 9. Estimated *f*-ratios at the primary production stations. Values shown include those calculated using only the measured rates of NO_3^- and NH_4^+ uptake (*f*-ratio$_{measured}$; Equation 5; background light blue bars), those calculated after accounting for mixed-layer nitrification (*f*-ratio; Equation 6; medium blue bars), and those subsequently calculated assuming that the "missing" N source was entirely new (*f*-ratio$_{new}$; Equation 7; white bars) or entirely regenerated (*f*-ratio$_{reg}$; Equation 8; dark blue bars). We take *f*-ratio$_{reg}$ as the most appropriate estimate of the Cape Basin *f*-ratios at the time of our sampling (see text for details). Eddy stations are indicated on the *x*-axis by the red boxes. Values of *f*-ratio$_{new}$ and *f*-ratio$_{reg}$ are not shown for Station 3 where net primary production was not measured, and only *f*-ratio$_{measured}$ is shown for Station 22 because we have no estimates of mixed-layer nitrification from the Benguela.

measurements (e.g., Newell et al., 2013; Peng et al., 2016; Sutka et al., 2004) including from a transect of the central North and South Atlantic (1–30 nmol L^{-1} d^{-1}; Clark et al., 2008). Additionally, elevated rates of NO_2^- oxidation were observed in the mixed layers of the Agulhas eddy stations but not outside these features (Figure 8). The assumption that all NO_3^- consumed by phytoplankton in the mixed layer is supplied by vertical mixing is problematic if nitrification occurs coincidentally since the NO_3^- produced therefrom constitutes a regenerated rather than a new form of N. Failure to account for phytoplankton consumption of regenerated NO_3^- will result in the overestimation of new and export production (Dugdale & Goering, 1967; Yool et al., 2007), and thus the strength of the biological pump.

Nitrification was historically disregarded as an important NO_3^- production pathway in the surface layer due to the evidence that nitrifiers are easily photo-inhibited (Hooper & Terry, 1974; Horrigan, 1981; Olson, 1981; Schön & Engel, 1962), coupled with the fact that they are outcompeted by phytoplankton for NH_4^+ (Smith et al., 2014; Ward, 2005; Zakem et al., 2018). These two drivers should restrict nitrifiers to the waters below the euphotic zone where NH_4^+ is readily supplied via bacterial remineralization of sinking organic matter and phytoplankton activity is light-limited. However, the scenario becomes more complicated when the MLD is similar to or deeper than z_{eu} since (a) phytoplankton will spend considerable time in low- to zero-light waters and thus be less competitive for NH_4^+ and (b) nitrifiers will be less photo-inhibited. Under these conditions, NO_3^- production by nitrifiers and its consumption by phytoplankton will overlap. Such a scenario has been observed in the central North and South Atlantic and North Pacific subtropical gyres where nitrification at times contributes >50% of the NO_3^- assimilated by phytoplankton (Clark et al., 2008; Shiozaki et al., 2016), as well as in the Southern Ocean in winter where >100% of photosynthetic NO_3^- assimilation has been shown to be supported by regenerated NO_3^- (Mdutyana et al., 2020, 2022; Smart et al., 2015).

At the edges of E1, mixed-layer NO_2^- oxidation equated to 31% (Station 15) and 4% (Station 19) of the photosynthetic NO_3^- uptake rate, increasing at the eddy center to 116% (Station 2) and 188% (Station 16). At the *CB background* and *SSA gyre* stations, NO_2^- oxidation contributed 35% (Station 12) and 3% (Station 7) of the NO_3^- consumed by phytoplankton (Table S2 and Text S1 in Supporting Information S1). The ratio of regenerated NO_3^- production to phytoplankton NO_3^- consumption was thus highest at the stations near the center of Agulhas eddies. We propose that the very deep mixed layers characteristic of these features favor nitrification, which not only occurred at higher absolute rates within the eddies but also contributed a far greater fraction of the NO_3^- consumed by phytoplankton compared to in the surrounding CB. Additionally,

and consistent with previous observations (Laperriere et al., 2021; Peng et al., 2018; Shiozaki et al., 2016), the ratio of nitrification to NO_3^- uptake was proportionally higher when NPP was lower. This finding may be expected given that a primary determinant of the relative importance of mixed-layer nitrification is light, which also exerts a strong control on NPP. Our observations imply that high regenerated NO_3^- production in Agulhas eddies driven by low average mixed-layer light availability, a condition that arises because of MLDs that extend beneath z_{eu} where the nitrification rates are highest, decreases new production in the CB and weakens its biological pump. This effect is superimposed on already-reduced rates of NO_3^- uptake and NPP at the eddy centers. By contrast, if the MLDs at eddy edges are shallow enough, they may not incorporate the maximum rates of nitrification that occur below the z_{eu} (e.g., see Station 19 in Figure 8). Additionally, the rates of both NPP and NO_3^- uptake are high at the eddy edges, rendering the relative supply of NO_3^- via nitrification even less significant.

Our study was conducted in winter when Agulhas eddy MLDs reach a maximum due to atmospheric heat loss that drives deep convective mixing (Duncombe Rae, 1991; Olson et al., 1990). In summer, shallower mixed layers are observed (on the order of 100–150 m; Duncombe Rae, 1991, 1992; Rigg, 1995), such that mixed-layer nitrification may be less important. However, NPP and NO_3^- uptake should also decline in summer when surface stratification impedes the upward supply of subsurface nutrients. It is thus alternately possibly that nitrification will continue to supply a significant fraction of the NO_3^- consumed by phytoplankton in Agulhas eddies in summer regardless of the absolute nitrification rate. Additionally, because of their anticyclonic circulation, Agulhas eddies tend to be characterized by deeper mixed layers than the rest of the CB throughout the year, so that even when the mixed layer shoals in summer, the likelihood of nitrification contributing a significant flux of regenerated NO_3^- to phytoplankton remains higher for the eddies than for background South Atlantic waters.

4.2.2. Other N Cycle Processes

Along with euphotic zone nitrification, forms of DON such as urea can be an important source of regenerated N to phytoplankton (Bronk, 2002). By contrast, N_2 fixation and atmospheric N deposition can supply new N to surface waters to augment the upward supply of subsurface NO_3^- (Capone et al., 2005; Owens et al., 1992). Multiplying our measured $\rho NO_3^- + \rho NH_4^+$ at the primary production stations (excluding Station 22) by the C:N ratio of ∼106:16 expected for phytoplankton undergoing balanced growth (Redfield, 1934) indicates that on average, NO_3^- plus NH_4^+ supported only 67% ± 14% of the NPP occurring across the transect (Figure 7b). The implication is that a significant proportion of NPP was fueled by an N source not measured in our study (Flynn et al., 2018; Mdutyana et al., 2020; Peng et al., 2018). This "missing" N could be new or regenerated, or a combination thereof, with varying implications for carbon export.

To the best of our knowledge, there are no estimates of N_2 fixation from the southern Benguela upwelling system or CB. However, measurements from the northern Benguela indicate that this flux is low (<1.5 nmol N L^{-1} d^{-1}) (Sohm et al., 2011; Wasmund et al., 2015) despite the excess phosphorous relative to N available in surface waters that should favor N_2 fixation (Deutsch et al., 2007; Flohr et al., 2014; Marshall et al., 2022). Low rates of N_2 fixation in the South Atlantic have been attributed to iron limitation of N_2 fixing phytoplankton (Moore et al., 2009) since the aeolian iron flux is more than a hundred-fold lower than in the North Atlantic (Sarthou et al., 2003) where N_2 fixation rates are high (Hood & Coles, 2007; Landolfi et al., 2018; Marconi et al., 2017). Equivalent biogeochemical conditions (i.e., excess phosphorus but low iron concentrations) characterize the southern Benguela and CB (Flynn et al., 2020), leading us to conclude that N_2 fixation is unlikely to account for the large flux of missing N. Similarly, modeling studies suggest that atmospheric N deposition to the southeastern Atlantic should be very low (Baker et al., 2010), although this flux has never been directly measured.

A more likely source of the missing N is an unmeasured form (or forms) of DON. The DON pool includes a myriad of compounds of varying lability and turnover time that are difficult to measure directly (Bronk, 2002; Clark et al., 2008). Nonetheless, DON can constitute the largest fixed N pool in surface waters, particularly in low-nutrient regions (Bronk, 2002). Urea has been shown to be a significant (albeit highly variable) source of N to phytoplankton in the southern Benguela (Probyn, 1990) and to at times contribute >50% of phytoplankton N in other ocean regions (Glibert et al., 1991; Peng et al., 2018; Varela et al., 2005). Additionally, other forms of DON such as dissolved free amino acids have been observed to fuel 30%–80% of marine phytoplankton growth under some conditions (Benner et al., 1997; Berg et al., 2001). It is thus likely that an average of 33% ± 14% of the NPP measured across our transect was supported by forms of regenerated DON such as urea, which in a mass-balance sense would yield no net carbon export (Dugdale & Goering, 1967).

4.3. Potential for Carbon Export Across the Cape Basin

The f-ratio$_{measured}$ at each primary production station was corrected for euphotic zone nitrification according to Equation 6 (f-ratio; intermediate blue bars in Figure 9). Given that ρNO_3^- + ρNH_4^+ did not fully support the measured NPP, we further revise our f-ratio estimates by considering two possible sources of missing N: (a) a new N source such as N_2 fixation or atmospheric N deposition (f-ratio$_{new}$; Equation 7; white bars in Figure 9) or (b) a regenerated N source such as DON (f-ratio$_{reg}$; Equation 8; dark blue bars in Figure 9). The revised f-ratios were calculated as follows (Table S2 and Text S1 in Supporting Information S1):

$$f-\text{ratio}_{\text{new}} = \frac{\left(\rho NO_3^- - NO_{2\,\text{revised}}^-\right) + \rho N_{\text{missing}}}{\left(\rho NO_3^- + \rho NH_4^+\right) + \rho N_{\text{missing}}} \tag{7}$$

$$f-\text{ratio}_{\text{reg}} = \frac{\left(\rho NO_3^- - NO_{2\,\text{revised}}^-\right)}{\left(\rho NO_3^- + \rho NH_4^+\right) + \rho N_{\text{missing}}} \tag{8}$$

Where the rate of missing N uptake ($\rho N_{missing}$) was estimated as:

$$\rho N_{\text{missing}} = \text{NPP} \times \left(\frac{16}{106}\right) - \left(\rho NO_3^- + \rho NH_4^+\right) \tag{9}$$

Accounting for newly nitrified NO_3^- decreased the f-ratio$_{measured}$ at the Open Ocean stations from an average of 0.62 ± 0.11 to 0.28 ± 0.26, with the most significant decline recorded in the center of E1 and in E2 (Stations 2, 16, and 11; f-ratio of 0; Figure 9). If we subsequently assume that the missing N was entirely new to the euphotic zone, we compute values of f-ratio$_{new}$ that, except at Station 16 where the nitrification rate was very high, exceed those calculated from ρNO_3^- and ρNH_4^+ only (average f-ratio$_{new}$ of 0.51 ± 0.24). However, as outlined above, it is highly unlikely that the missing N source was new to the euphotic zone given the lack of evidence for significant rates of N_2 fixation or atmospheric N deposition.

Accounting for a missing flux of regenerated N reduces the average f-ratio across the transect (i.e., f-ratio$_{reg}$) to 0.22 ± 0.21, within the range (albeit at the high end) of estimates from other oligotrophic regions (Eppley & Peterson, 1979; Lipschultz, 2001). At the center of E1, f-ratio$_{reg}$ was 0, indicating that NPP was fueled exclusively by regenerated N and carbon export potential was zero. Within E1, the highest f-ratio$_{reg}$ was estimated for Station 19 at its eastern edge (0.64), followed by the neighboring Station 18 (0.30). A high f-ratio$_{reg}$ was also computed for Station 5 in E3 (0.24). At the non-eddy Stations 12 and 7, f-ratio$_{reg}$ was 0.27 and 0.29, respectively. Our calculations suggest that Agulhas eddy edges support higher carbon export potential, while diminished rates of export production occur in the center of the eddies. We propose that light limitation of phytoplankton in the eddy centers not only favors regenerated NO_3^- production by nitrifiers, but also drives proportionally greater phytoplankton reliance on regenerated N forms (NH_4^+ and DON) that are less energetically expensive to assimilate than NO_3^- (Dortch, 1990). At the same time, enhanced productivity and carbon export potential at the eddy edges may at least partially offset the dampening of productivity that occurs at the eddy centers.

5. Summary and Concluding Remarks

The net effect of Agulhas eddies on CB productivity is difficult to quantify given the hydrodynamic complexity of the region and the synoptic nature of our study. Additional research focused on the effect(s) of Agulhas leakage on carbon production and export in the South Atlantic is thus clearly needed. Nonetheless, our high-resolution sampling of E1 yields new insights into the influence of Agulhas leakage on carbon production and export potential in the South Atlantic. In general, large variations in MLD (and thus the light available to phytoplankton) appear to dampen total and new production at Agulhas eddy centers but enhance it at their edges, with productivity increasing further at the eddy edges when nutrients are injected into surface waters via submesoscale physical processes, as occurred at the eastern edge of E1. Our results thus suggest that while anticyclonic Agulhas eddies are unproductive at their centers, the perturbations that they induce as they transit the CB can elevate productivity at their edges, which may partly offset the downwelling-related decline in production at their centers. To more fully probe the changes in productivity that occur at Agulhas eddy edges and centers relative to the background state, we suggest that future studies include high-resolution sampling of Agulhas eddies on an evenly spaced horizontal grid.

The highest integrated rates of nitrification were measured at the center of E1, with enough regenerated NO_3^- produced to support all NO_3^--based phytoplankton growth in the euphotic zone. Given these high nitrification rates, approximating the *f*-ratio across the CB by equating NO_3^- and NH_4^+ uptake to new and regenerated production vastly overestimates the fraction of potentially exportable carbon. Another source of uncertainty is the extent to which unmeasured N sources, particularly regenerated DON forms, fuel NPP; we estimate that DON supported approximately a third of NPP at the time of our sampling. Future studies of CB productivity should include direct measurements of DON uptake (and possibly also N_2 fixation), and should additionally consider seasonality.

Eddies traveling into the CB are highly energetic, interacting vigorously with their background environment and with one another (Richardson et al., 2003). The SLA data show that E1, E2, and E3 existed at least six months prior to our study (Figure S1 in Supporting Information S1). Between the time of their formation and our sampling, all three eddies underwent significant merging, splitting, and warping, which are well-documented phenomena in the CB that ultimately produce vortices of varying shapes and sizes that can behave very differently (Arhan & Mercier, 1999; Laxenaire et al., 2018). Our data suggest that the physical disturbances induced by the passage of Agulhas eddies have a greater effect on CB productivity than the biological and/or biogeochemical properties transported by these eddies. This notion is consistent with the fairly recent consideration of eddy mesoscale in ocean models and observations, which has increased estimates of NPP in the oligotrophic ocean by 30% (Mahadevan & Archer, 2000; Oschlies & Garçon, 1998; Spall & Richards, 2000). Modeling studies have also shown that submesoscale frontal jets and filaments generated by ageostrophic dynamics associated with eddy-eddy interactions further increase the vertical nutrient supply, enhancing phytoplankton biomass and raising NPP by as much as 100% (Lévy et al., 2001; Spall & Richards, 2000).

Because of our sampling design, we have emphasized the mesoscale response of CB productivity to the passage of an Agulhas eddy. However, submesoscale dynamics almost certainly also influenced the biogeochemical signals that we observed, with the isopycnal shoaling and associated nutrient injection at the eastern edge of E1 epitomizing such dynamics. As rings and eddies age and travel away from, assuming they do not dissipate in the CB, they are subject to progressively less submesoscale activity, which allows them to stratify and become more stable (Lutjeharms & Gordon, 1987; Schouten et al., 2000). As such, while it is important that we improve our understanding of the effects of submesoscale eddy-related processes on nutrient and phytoplankton transport, as well as on the biogeochemical responses in the eddies and their surrounds, there remains considerable value in studying eddies at the mesoscale.

Acknowledgments
We thank the Captain and crew of the R/V *SA Agulhas II* and the Department of Forestry, Fisheries and Environment (DFFE): Oceans and Coasts, particularly M. van den Berg who acted as Chief Scientist during the cruise. We also thank K. Spence and R. Granger for assistance at sea, I. Newton and K. Pescok Ewert for isotope measurements, and the Marine Biogeochemistry Lab at the University of Cape Town (UCT). This research was supported by the South African Department of Science and Innovation (DSI) through their SEAmester programme (seamester.co.za), the South African National Research Foundation (NRF) through Grant 129229 to IJA and M. van den Berg; 112380 to MM; and 129320 and 116142 to SEF, UCT through postgraduate awards to SW, RGP, and HJF, a Harry Crossley Foundation Research Fellowship to MM, and a VC Future Leaders 2030 award and Research Committee Equipment grant to SEF, and by the African Academy of Sciences/Royal Society through a FLAIR Fellowship to SEF. The authors also acknowledge the DSI's Biogeochemistry Research Infrastructure Platform (BIOGRIP; www.biogrip.ac.za). Figures 2 and 4 in the main text and Figure S2 in Supporting Information S1 were made using Ocean DataView (ODV) (Schlitzer, 2016).

Data Availability Statement

The data discussed in this paper are available in the Zenodo database and can be found at https://doi.org/10.5281/zenodo.6629428.

References

Andrews, W. R. H., & Hutchings, L. (1980). Upwelling in the southern Benguela Current. *Progress in Oceanography*, *9*(1), 1–8. https://doi.org/10.1016/0079-6611(80)90015-4

Ansorge, I. J., Baringer, M. O., Campos, E. J. D., Dong, S., Fine, R. A., Garzoli, S. L., et al. (2014). Basin-wide oceanographic array bridges the South Atlantic. *Eos*, *95*(6), 53–54. https://doi.org/10.1002/2014EO060001

Arhan, M., Mercier, H., & Lutjeharms, J. R. E. (1999). The disparate evolution of three Agulhas rings in the South Atlantic Ocean. *Journal of Geophysical Research*, *104*(C9), 20987–21005. https://doi.org/10.1029/1998jc900047

Baker, A. R., Lesworth, T., Adams, C., Jickells, T. D., & Ganzeveld, L. (2010). Estimation of atmospheric nutrient inputs to the Atlantic Ocean from 50°N to 50°S based on large-scale field sampling: Fixed nitrogen and dry deposition of phosphorus. *Global Biogeochemical Cycles*, *24*(7), GB3006. https://doi.org/10.1029/2009GB003634

Bang, N. D. (1970). Dynamic interpretations of a detailed surface temperature chart of the Agulhas Current retroflexion and fragmentation area. *South African Geographical Journal*, *52*(1), 67–76. https://doi.org/10.1080/03736245.1970.10559466

Beal, L. M., De Ruijter, W. P. M., Biastoch, A., Zahn, R., Cronin, M., Hermes, J., et al. (2011). On the role of the Agulhas system in ocean circulation and climate. *Nature*, *472*(7344), 429–436. https://doi.org/10.1038/nature09983

Beal, L. M., Elipot, S., Houk, A., & Leber, G. M. (2015). Capturing the transport variability of a western boundary jet: Results from the Agulhas Current time-series experiment (ACT). *Journal of Physical Oceanography*, *45*(5), 1302–1324. https://doi.org/10.1175/JPO-D-14-0119.1

Benner, R., Biddanda, B., Black, B., & McCarthy, M. (1997). Abundance, size distribution, and stable carbon and nitrogen isotopic compositions of marine organic matter isolated by tangential-flow ultrafiltration. *Marine Chemistry*, *57*(3–4), 243–263. https://doi.org/10.1016/S0304-4203(97)00013-3

Bennett, S. L. (1988). Where three oceans meet: The Algulhas retroflection region [Massachusetts Institute of Technology]. In *Where three oceans meet: The Algulhas retroflection region*. https://doi.org/10.1575/1912/4761

Berg, G. M., Glibert, P. M., Jørgensen, N. O. G., Balode, M., & Purina, I. (2001). Variability in inorganic and organic nitrogen uptake associated with riverine nutrient input in the Gulf of Riga, Baltic Sea. *Estuaries*, *24*(2), 204–214. https://doi.org/10.2307/1352945

Boebel, O., Lutjeharms, J., Schmid, C., Zenk, W., Rossby, T., & Barron, C. (2003). The Cape Cauldron: A regime of turbulent inter-ocean exchange. *Deep-Sea Research Part II Topical Studies in Oceanography*, *50*(1), 57–86. https://doi.org/10.1016/S0967-0645(02)00379-X

Bronk, D. A. (2002). Dynamics of DON. In *Biogeochemistry of marine dissolved organic matter* (pp. 153–247). https://doi.org/10.1016/b978-012323841-2/50007-5

Bronk, D. A., Gilbert, P. M., & Ward, B. B. (1994). Nitrogen uptake, dissolved organic nitrogen release, and new production. *Science*, *265*(5180), 1843–1846. https://doi.org/10.1126/science.265.5180.1843

Bryden, H. L., Beal, L. M., & Duncan, L. M. (2005). Structure and transport of the Agulhas current and its temporal variability. *Journal of Oceanography*, *61*(3), 479–492. https://doi.org/10.1007/s10872-005-0057-8

Byrne, D. A., Gordon, A. L., & Haxby, W. F. (1995). Agulhas eddies: A synoptic view using Geosat ERM data. *Journal of Chemical Information and Modeling*, *25*(5), 902–917. https://doi.org/10.1175/1520-0485(1995)025<0902:AEASVU>2.0.CO;2

Capone, D. G., Burns, J. A., Montoya, J. P., Subramaniam, A., Mahaffey, C., Gunderson, T., et al. (2005). Nitrogen fixation by *Trichodesmium* spp.: An important source of new nitrogen to the tropical and subtropical North Atlantic Ocean. *Global Biogeochemical Cycles*, *19*(2), 1–17. https://doi.org/10.1029/2004GB002331

Capuano, T. A., Speich, S., Carton, X., & Blanke, B. (2018). Mesoscale and submesoscale processes in the southeast Atlantic and their impact on the regional thermohaline structure. *Journal of Geophysical Research: Oceans*, *123*(3), 1937–1961. https://doi.org/10.1002/2017JC013396

Carpenter, J. H. (1965). The accuracy of the winkler method for dissolved oxygen analysis. *Limnology and Oceanography*, *10*(1), 135–140. https://doi.org/10.4319/lo.1965.10.1.0135

Chelton, D. B., Schlax, M. G., & Samelson, R. M. (2011). Global observations of nonlinear mesoscale eddies. *Progress in Oceanography*, *91*(2), 167–216. https://doi.org/10.1016/j.pocean.2011.01.002

Clark, D. R., Rees, A. P., & Joint, I. (2008). Ammonium regeneration and nitrification rates in the oligotrophic Atlantic Ocean: Implications for new production estimates. *Limnology and Oceanography*, *53*(1), 52–62. https://doi.org/10.4319/lo.2008.53.1.0052

D'Ovidio, F., Monte, S. D., Penna, A. D., Cotté, C., & Guinet, C. (2013). Ecological implications of eddy retention in the open ocean: A Lagrangian approach. *Journal of Physics A: Mathematical and Theoretical*, *46*(25), 254023. https://doi.org/10.1088/1751-8113/46/25/254023

Daher, H., Beal, L. M., & Schwarzkopf, F. U. (2020). A new improved estimation of Agulhas leakage using observations and simulations of Lagrangian floats and drifters. *Journal of Geophysical Research: Oceans*, *125*(4), 1–17. https://doi.org/10.1029/2019JC015753

de Boyer Montégut, C., Madec, G., Fischer, A. S., Lazar, A., & Iudicone, D. (2004). Mixed layer depth over the global ocean: An examination of profile data and a profile-based climatology. *Journal of Geophysical Research*, *109*(12), 1–20. https://doi.org/10.1029/2004JC002378

De La Rocha, C., & Passow, U. (2014). The biological pump. In H. D. Holland & K. K. Turekian (Eds.), *Treatise on geochemistry* (2nd ed., pp. 93–122). Elsevier Science. https://doi.org/10.1016/B978-0-08-095975-7.00604-5

Denman, K. L., & Gargett, A. E. (1983). Time and space scales of vertical mixing and advection of phytoplankton in the upper ocean. *Limnology and Oceanography*, *28*(5), 801–815. https://doi.org/10.4319/lo.1983.28.5.0801

De Ruijter, W. P. M., Biastoch, A., Drijfhout, S. S., Lutjeharms, J. R. E., Matano, R. P., Pichevin, T., et al. (1999). Indian-Atlantic interocean exchange: Dynamics, estimation and impact. *Journal of Geophysical Research*, *104*(C9), 20885–20910. https://doi.org/10.1029/1998jc900099

Deutsch, C., Sarmiento, J. L., Sigman, D. M., Gruber, N., & Dunne, J. P. (2007). Spatial coupling of nitrogen inputs and losses in the ocean. *Nature*, *445*(7124), 163–167. https://doi.org/10.1038/nature05392

Diaz, F., & Raimbault, P. (2000). Nitrogen regeneration and dissolved organic nitrogen release during spring in a NW Mediterranean coastal zone (Gulf of Lions): Implications for the estimation of new production. *Marine Ecology Progress Series*, *197*, 51–65. https://doi.org/10.3354/meps197051

Donners, J., & Drijfhout, S. S. (2004). The Lagrangian view of South Atlantic interocean exchange in a global ocean model compared with inverse model results. *Journal of Physical Oceanography*, *34*(5), 1019–1035. https://doi.org/10.1175/1520-0485(2004)034<1019:TLVOSA>2.0.CO;2

Dortch, Q. (1990). The interaction between ammonium and nitrate uptake in phytoplankton. *Marine Ecology Progress Series*, *61*, 183–201. https://doi.org/10.3354/meps061183

Dower, K. M., & Lucas, M. I. (1993). Photosynthesis-irradiance relationships and production associated with a warm-core ring shed from the Agulhas Retroflection south of Africa. *Marine Ecology Progress Series*, *95*(1–2), 141–154. https://doi.org/10.3354/meps095141

Dufois, F., Hardman-Mountford, N. J., Greenwood, J., Richardson, A. J., Feng, M., Herbette, S., & Matear, R. (2014). Impact of eddies on surface chlorophyll in the South Indian Ocean. *Journal of Geophysical Research: Oceans*, *199*(111), 8061–8077. https://doi.org/10.1002/2014JC010164. Received

Dufois, F., Hardman-Mountford, N. J., Greenwood, J., Richardson, A. J., Feng, M., & Matear, R. J. (2016). Anticyclonic eddies are more productive than cyclonic eddies in subtropical gyres because of winter mixing. *Science Advances*, *2*(5), 1–7. https://doi.org/10.1126/sciadv.1600282

Dugdale, R. C., & Goering, J. J. (1967). Uptake of new and regenerated forms of nitrogen in primary productivity. *Limnology and Oceanography*, *12*(2), 196–206. https://doi.org/10.4319/lo.1967.12.2.0196

Dugdale, R. C., & Wilkerson, F. P. (1986). The use of 15°N to measure nitrogen uptake; experimental considerations. *Limnology and Oceanography*, *31*(4), 673–689. https://doi.org/10.4319/lo.1986.31.4.0673

Duncombe Rae, C. M. (1991). Agulhas retroflection rings in the south Atlantic Ocean: An overview. *South African Journal of Marine Science*, *11*(1), 327–344. https://doi.org/10.2989/025776191784287574

Duncombe Rae, C. M., Shillington, F. A., Agenbag, J. J., Taunton-Clark, J., & Gründlingh, M. L. (1992). An Agulhas ring in the South Atlantic ocean and its interaction with the Benguela upwelling frontal system. *Deep-Sea Research, Part A: Oceanographic Research Papers*, *39*(11–12), 2009–2027. https://doi.org/10.1016/0198-0149(92)90011-H

Egan, L. (2008). Determination of nitrate and/or nitrite in brackish or seawater by flow injection analysis QuikChem method 31-107-04-1-C. In *Lachat Instruments*.

Eppley, R. W., & Peterson, B. J. (1979). Particulate organic matter flux and planktonic new production in the deep ocean. *Nature*, *282*(5740), 677–680. https://doi.org/10.1038/282677a0

Falkowski, P. G., Ziemann, D., Kolber, Z., & Bienfang, P. K. (1991). Role of eddy pumping in enhancing primary productivity. *Nature*, *354*, 56–58.

Flierl, G., & McGillicuddy, D. J. (2002). Mesoscale and submesoscale physical-biological interactions. *The Sea*, *12*, 113–185.

Flierl, G. R. (1981). Particle motions in large-amplitude wave fields. *Geophysical & Astrophysical Fluid Dynamics*, *18*(1–2), 39–74. https://doi.org/10.1080/03091928108208773

Flohr, A., Van Der Plas, A. K., Emeis, K. C., Mohrholz, V., & Rixen, T. (2014). Spatio-temporal patterns of C: N: P ratios in the northern Benguela upwelling system. *Biogeosciences*, *11*(3), 885–897. https://doi.org/10.5194/bg-11-885-2014

Flynn, R. F., Burger, J. M., Pillay, K., & Fawcett, S. E. (2018). Wintertime rates of net primary production and nitrate and ammonium uptake in the southern Benguela upwelling system. *African Journal of Marine Science*, *40*(3), 253–266. https://doi.org/10.2989/1814232X.2018.1502095

Flynn, R. F., Granger, J., Veitch, J. A., Siedlecki, S., Burger, J. M., Pillay, K., & Fawcett, S. E. (2020). On-shelf nutrient trapping enhances the fertility of the southern Benguela upwelling system. *Journal of Geophysical Research: Oceans*, *125*(6), 1–19. https://doi.org/10.1029/2019JC015948

Glibert, P. M., Garside, C., Fuhrman, J. A., & Roman, M. R. (1991). Dependent coupling of inorganic and organic nitrogen uptake and regeneration in the plume of the Chesapeake Bay estuary and its regulation by large heterotrophs. *Limnology and Oceanography*, *36*(5), 895–909. https://doi.org/10.4319/lo.1991.36.5.0895

Gordon, A. L. (1985). Indian-Atlantic transfer of thermocine water at the Agulhas retroflection. *Science*, *227*(4690), 1030–1033. https://doi.org/10.1126/science.227.4690.1030

Gordon, A. L., Lutjeharms, J. R. E., & Gründlingh, M. L. (1987). Stratification and circulation at the Agulhas retroflection. *Deep-Sea Research, Part A: Oceanographic Research Papers*, *34*(4), 565–599. https://doi.org/10.1016/0198-0149(87)90006-9

Gordon, A. L., Weiss, R., Smethie, W. M., & Warner, M. J. (1992). Thermocline and intermediate water communication. *Journal of Geophysical Research*, *97*(92), 7223–7240. https://doi.org/10.1029/92JC00485

Gordon, H. R., Clark, D. K., Brown, J. W., Brow, O. B., & Evans, R. H. (1982). Satellite measurement of the phytoplankton pigment concentration in the surface waters of a warm core Gulf Stream ring. *Journal of Marine Research*, *40*(2), 491–502.

Gould, R. W., & Fryxell, G. A. (1988). Phytoplankton species composition and abundance in a Gulf Stream warm core ring. II. Distributional patterns. *Journal of Marine Research*, *46*(2), 399–428. https://doi.org/10.1357/002224088785113612

Granger, J., & Sigman, D. M. (2009). Removal of nitrite with sulfamic acid for nitrate N and O isotope analysis with the denitrifier method. *Rapid Communications in Mass Spectrometry*, *23*(23), 3753–3762. https://doi.org/10.1002/rcm.4307

Grasshoff, K., Ehrhardt, M., Kremling, K., Almgren, T., & Ehrhardt, M. (1983). Methods of seawater analysis.

Hall, C., & Lutjeharms, J. R. E. (2010). Cyclonic eddies identified in the Cape Basin of the south Atlantic Ocean. *Journal of Marine Systems*, *85*(1–2), 1–10. https://doi.org/10.1016/j.jmarsys.2010.10.003

Harris, G. P. (1980). Temporal and spatial scales in phytoplankton ecology. Mechanisms, methods, models, and management. *Canadian Journal of Fisheries and Aquatic Sciences*, *37*(5), 877–900. https://doi.org/10.1139/f80-117

Harrison, W. G. (1978). Experimental measurements of nitrogen remineralization in coastal waters. *Limnology and Oceanography*, *23*(4), 684–694. https://doi.org/10.4319/lo.1978.23.4.0684

Hitchcock, G. L., Langdon, C., & Smayda, T. J. (1985). Seasonal variations in the phytoplankton biomass and productivity of a warm-core Gulf Stream ring. *Deep-Sea Research, Part A: Oceanographic Research Papers*, *32*(11), 1287–1300. https://doi.org/10.1016/0198-0149(85)90049-4

Holligan, P., Williams, P., Purdie, D., & Harris, R. (1984). Photosynthesis, respiration and nitrogen supply of plankton populations in stratified, frontal and tidally mixed shelf waters. *Marine Ecology Progress Series*, *17*(2), 201–213. https://doi.org/10.3354/meps017201

Holmes, R. M., Aminot, A., Kérouel, R., Hooker, B. A., & Peterson, B. J. (1999). A simple and precise method for measuring ammonium in marine and freshwater ecosystems. *Canadian Journal of Fisheries and Aquatic Sciences*, *56*(10), 1801–1808. https://doi.org/10.1139/f99-128

Holton, L., Deshayes, J., Backeberg, B. C., Loveday, B. R., Hermes, J. C., & Reason, C. J. C. (2017). Spatio-temporal characteristics of Agulhas leakage: A model inter-comparison study. *Climate Dynamics*, *48*(7–8), 2107–2121. https://doi.org/10.1007/s00382-016-3193-5

Hood, R. R., & Coles, V. J. (2007). Modeling the impact of iron and phosphorus limitations on nitrogen fixation inthe Atlantic Ocean. *Biogeosciences*, *4*(4), 455–479. https://doi.org/10.5194/bg-4-455-2007

Hooper, A. B., & Terry, K. R. (1974). Photoinactivation of ammonia oxidation in Nitrosomonas. *Journal of Bacteriology*, *119*(3), 899–906. https://doi.org/10.1128/jb.119.3.899-906.1974

Horak, R. E. A., Qin, W., Schauer, A. J., Armbrust, E. V., Ingalls, A. E., Moffett, J. W., et al. (2013). Ammonia oxidation kinetics and temperature sensitivity of a natural marine community dominated by Archaea. *The ISME Journal*, *7*(10), 2023–2033. https://doi.org/10.1038/ismej.2013.75

Horrigan, S. G. (1981). Primary production under the Ross Ice Shelf, Antarctica. *Limnology and Oceanography*, *26*(2), 378–382. https://doi.org/10.4319/lo.1981.26.2.0378

Hydes, D., Aoyama, M., Aminot, A., Bakker, K., Becker, S., Coverly, S., et al. (2010). Determination of dissolved nutrients (N, P, Si) in seawater with high precision and inter-comparability using gas-segmented continuous flow analysers. The GO-SHIP repeat hydrography manual: A collection of expert reports and guidelines. IOCCP report no.14. In *The GO-SHIP repeat hydrography manual IOCCP report* (pp. 1–87).

Landolfi, A., Kähler, P., Koeve, W., & Oschlies, A. (2018). Global marine N_2 fixation estimates: From observations to models. *Frontiers in Microbiology*, *9*(September), 1–8. https://doi.org/10.3389/fmicb.2018.02112

Laperriere, S. M., Morando, M., Capone, D. G., Gunderson, T., Smith, J. M., & Santoro, A. E. (2021). Nitrification and nitrous oxide dynamics in the Southern California Bight. *Limnology and Oceanography*, *66*(4), 1099–1112. https://doi.org/10.1002/lno.11667

Laxenaire, R., Speich, S., Blanke, B., Chaigneau, A., Pegliasco, C., & Stegner, A. (2018). Anticyclonic eddies connecting the Western boundaries of Indian and Atlantic Oceans. *Journal of Geophysical Research: Oceans*, *123*(11), 7651–7677. https://doi.org/10.1029/2018JC014270

Lehahn, Y., D'Ovidio, F., Lévy, M., Amitai, Y., & Heifetz, E. (2011). Long range transport of a quasi isolated chlorophyll patch by an Agulhas ring. *Geophysical Research Letters*, *38*(16), 1–6. https://doi.org/10.1029/2011GL048588

Lévy, M., Klein, P., & Treguier, A. M. (2001). Impact of sub-mesoscale physics on production and subduction of phytoplankton in an oligotrophic regime. *Journal of Marine Research*, *59*(4), 535–565. https://doi.org/10.1357/002224001762842181

Lévy, M., Mémery, L., & Madec, G. (1998). The onset of a bloom after deep winter convection in the northwestern Mediterranean sea: Mesoscale process study with a primitive equation model. *Journal of Marine Systems*, *16*(1–2), 7–21. https://doi.org/10.1016/S0924-7963(97)00097-3

Lévy, M., Mémery, L., & Madec, G. (1999). The onset of the Spring Bloom in the MEDOC area: Mesoscale spatial variability. *Deep-Sea Research Part I Oceanographic Research Papers*, *46*(7), 1137–1160. https://doi.org/10.1016/S0967-0637(98)00105-8

Lima, I. D., Olson, D. B., & Doney, S. C. (2002). Biological response to frontal dynamics and mesoscale variability in oligotrophic environments: Biological production and community structure. *Journal of Geophysical Research*, *107*(8), 1–21. https://doi.org/10.1029/2000jc000393

Lipschultz, F. (2001). A time-series assessment of the nitrogen cycle at BATS. *Deep-Sea Research Part II Topical Studies in Oceanography*, *48*(8–9), 1897–1924. https://doi.org/10.1016/S0967-0645(00)00168-5

Lovecchio, E., Gruber, N., Münnich, M., & Frenger, I. (2022). On the processes sustaining biological production in the offshore propagating eddies of the northern Canary Upwelling System. *Journal of Geophysical Research: Oceans*, *127*(2), 1–28. https://doi.org/10.1029/2021JC017691

Lutjeharms, J. R. E. (1981). Features of the southern Agulhas Current circulation from satellite remote sensing. *South African Journal of Science*, *77*, 231–236. https://doi.org/10.10520/AJA00382353_1526

Lutjeharms, J. R. E. (2006). *The Agulhas current retroflection* (pp. 151–207). Springer Berlin Heidelberg.

Lutjeharms, J. R. E., & Cooper, J. (1996). Interbasin leakage through Agulhas current filaments. *Deep-Sea Research Part I Oceanographic Research Papers*, *43*(2), 213–215. https://doi.org/10.1016/0967-0637(96)00002-7

Lutjeharms, J. R. E., & Gordon, A. L. (1987). Shedding of an Agulhas ring observed at sea. *Nature*, *325*(6100), 138–140. https://doi.org/10.1038/325138a0

Lutjeharms, J. R. E., & van Ballegooyen, R. C. (1984). Topographic control in the Agulhas current system. *Deep-Sea Research, Part A: Oceanographic Research Papers*, *31*(11), 1321–1337. https://doi.org/10.1016/0198-0149(84)90004-9

Lutjeharms, J. R. E., & van Ballegooyen, R. C. (1988). The retroflection of the Agulhas current. *Journal of Physical Oceanography*, *18*(11), 1570–1583. https://doi.org/10.1175/1520-0485(1988)018<1570:trotac>2.0.co;2

Mahadevan, A. (2016). The impact of submesoscale physics on primary productivity of plankton. *Annual Review of Marine Science*, *8*(September), 161–184. https://doi.org/10.1146/annurev-marine-010814-015912

Mahadevan, A., & Archer, D. (2000). Modeling the impact of fronts and mesoscale circulation on the nutrient supply and biogeochemistry of the upper ocean. *Journal of Geophysical Research*, *105*(C1), 1209–1225. https://doi.org/10.1029/1999jc900216

Mahadevan, A., Thomas, L. N., & Tandon, A. (2008). Comment on "eddy/wind interactions stimulate extraordinary mid-ocean plankton blooms. *Science*, *320*(5875), 448. https://doi.org/10.1126/science.1152111

Marconi, D., Sigman, D. M., Casciotti, K. L., Campbell, E. C., Alexandra Weigand, M., Fawcett, S. E., et al. (2017). Tropical dominance of N_2 fixation in the north Atlantic Ocean. *Global Biogeochemical Cycles*, *31*(10), 1608–1623. https://doi.org/10.1002/2016GB005613

Marshall, T., Granger, J., Casciotti, K. L., Dähnke, K., Emeis, K. C., Marconi, D., et al. (2022). The Angola Gyre is a hotspot of dinitrogen fixation in the South Atlantic Ocean. *Communications Earth & Environment*, *3*(1), 1–10.

Martin, A. P. (2003). Phytoplankton patchiness: The role of lateral stirring and mixing. *Progress in Oceanography*, *57*(2), 125–174. https://doi.org/10.1016/s0079-6611(03)00085-5

Martin, A. P., & Richards, K. J. (2001). Mechanisms for vertical nutrient transport within a North Atlantic mesoscale eddy. *Deep-Sea Research Part II Topical Studies in Oceanography*, *48*(4–5), 757–773. https://doi.org/10.1016/S0967-0645(00)00096-5

McDonagh, E. L., & Heywood, K. J. (1999). The origin of an Anomalous ring in the southeast Atlantic. *Journal of Physical Oceanography*, *29*(8), 2050–2064. https://doi.org/10.1175/1520-0485(1999)029<2050:TOOAAR>2.0.CO;2

McGillicuddy, D. J. (2016). Mechanisms of physical-biological-biogeochemical interaction at the oceanic mesoscale. In *Annual review of marine science* (Vol. 8). https://doi.org/10.1146/annurev-marine-010814-015606

McGillicuddy, D. J., Anderson, L. A., Bates, N. R., Bibby, T., Buesseler, K. O., Carlson, C. A., et al. (2007). Eddy/wind interactions stimulate extraordinary mid-ocean plankton blooms. *Science*, *316*(May), 1021–1026. https://doi.org/10.1126/science.1136256

McGillicuddy, D. J., Robinson, A. R., & McCarthy, J. J. (1995). Coupled physical and biological modelling of the spring bloom in the north Atlantic (II): Three dimensional bloom and post-bloom processes. *Deep-Sea Research Part I*, *42*(8), 1359–1398. https://doi.org/10.1016/0967-0637(95)00035-5

Mdutyana, M., Marshall, T., Sun, X., Burger, J. M., Thomalla, S. J., & Fawcett, S. E. (2022). Controls on nitrite oxidation in the upper Southern Ocean: Insights from winter kinetics experiments in the Indian sector. *Biogeosciences*, *19*(14), 3425–3444. https://doi.org/10.5194/bg-2021-280

Mdutyana, M., Thomalla, S. J., Philibert, R., Ward, B. B., & Fawcett, S. E. (2020). The seasonal cycle of nitrogen uptake and nitrification in the Atlantic sector of the Southern Ocean. *Global Biogeochemical Cycles*, *34*(7), 1–29. https://doi.org/10.1029/2019GB006363

Mizobata, K., Saitoh, S. I., Shiomoto, A., Miyamura, T., Shiga, N., Imai, K., et al. (2002). Bering Sea cyclonic and anticyclonic eddies observed during summer 2000 and 2001. *Progress in Oceanography*, *55*(1–2), 65–75. https://doi.org/10.1016/S0079-6611(02)00070-8

Moore, M. C., Mills, M. M., Achterberg, E. P., Geider, R. J., Laroche, J., Lucas, M. I., et al. (2009). Large-scale distribution of Atlantic nitrogen fixation controlled by iron availability. *Nature Geoscience*, *2*(12), 867–871. https://doi.org/10.1038/ngeo667

Nelson, D. M., Ducklow, H. W., Hitchcock, G. L., Brzezinski, M. A., Cowles, T. J., Garside, C., et al. (1985). Distribution and composition of biogenic particulate matter in a Gulf Stream warm-core ring. *Deep-Sea Research, Part A: Oceanographic Research Papers*, *32*(11), 1347–1369. https://doi.org/10.1016/0198-0149(85)90052-4

Newell, S. E., Fawcett, S. E., & Ward, B. B. (2013). Depth distribution of ammonia oxidation rates and ammonia-oxidizer community composition in the Sargasso Sea. *Limnology and Oceanography*, *58*(4), 1491–1500. https://doi.org/10.4319/lo.2013.58.4.1491

Obernosterer, I., & Herndl, G. (1995). Phytoplankton extracellular release and bacterial growth: Dependence on the inorganic N:P ratio. *Marine Ecology Progress Series*, *116*(1–3), 247–257. https://doi.org/10.3354/meps116247

Olson, D., & Evans, R. (1986). Rings of the Agulhas Current. *Deep-Sea Research, Part A: Oceanographic Research Papers*, *33*(1), 27–42. https://doi.org/10.1016/0198-0149(86)90106-8

Olson, D., Fine, R., & Gordon, A. (1990). Convective modifications of water masses in the Agulhas. *Deep-Sea Research, Part A: Oceanographic Research Papers*, *39*, S163–S181. https://doi.org/10.1016/s0198-0149(11)80010-5

Olson, R. (1981). Differential photoinhibition of marine nitrifying bacteria: A possible mechanism for the formation of the primary nitrite maximum. *Journal of Marine Research*, *39*(2), 227–238.

Ortner, P. B., Ferguson, R. L., Piotrowicz, S. R., Chesal, L., Berberian, G., & Palumbo, A. V. (1984). Biological consequences of hydrographic and atmospheric advection within the Gulf Loop Intrusion. *Deep-Sea Research, Part A: Oceanographic Research Papers*, *31*(9), 1101–1120. https://doi.org/10.1016/0198-0149(84)90015-3

Oschlies, A., & Garçon, V. (1998). Eddy-influenced enhancement of primary production in a model of the North Atlantic Ocean. *Nature*, *394*(6690), 266–269. https://doi.org/10.1038/28373

Owens, N. J., Galloway, J. N., & Duce, R. A. (1992). Episodic atmospheric nitrogen deposition to oligotrophic oceans. *Nature*, *359*(8), 710–713. https://doi.org/10.1038/357397a0

Peng, X., Fawcett, S. E., van Oostende, N., Wolf, M. J., Marconi, D., Sigman, D. M., & Ward, B. B. (2018). Nitrogen uptake and nitrification in the subarctic North Atlantic Ocean. *Limnology and Oceanography*, *63*(4), 1462–1487. https://doi.org/10.1002/lno.10784

Peng, X., Fuchsman, C. A., Jayakumar, A., Oleynik, S., Martens-Habbena, W., Devol, A. H., & Ward, B. B. (2015). Ammonia and nitrite oxidation in the eastern tropical north Pacific. *Global Biogeochemical Cycles*, *29*(12), 2034–2049. https://doi.org/10.1111/1462-2920.13280

Peng, X., Fuchsman, C. A., Jayakumar, A., Warner, M. J., Devol, A. H., & Ward, B. B. (2016). Revisiting nitrification in the eastern tropical South Pacific: A focus on controls. *Journal of Geophysical Research: Oceans*, *121*(3), 1667–1684. https://doi.org/10.1002/2015JC011455.Received

Probyn, T. A. (1990). Size-fractionated measurements of nitrogen uptake in aged upwelled waters: Implications for pelagic food webs. *Limnology and Oceanography*, *35*(1), 202–210. https://doi.org/10.4319/lo.1990.35.1.0202

Provenzale, A. (1999). Transport by coherent barotrophic vortices. *Annual Review of Fluid Mechanics*, *31*(1), 55–93. https://doi.org/10.1146/annurev.fluid.31.1.55

Redfield, A. C. (1934). *On the proportions of organic derivatives in sea water and their relation to the composition of plankton* (Vol. 1). University Press of Liverpool. Retrieved from http://scholar.google.com/scholar?hl=en%26btnG=Search%26q=intitle:On+the+proportions+of+organic+derivatives+in+sea+water+and+their+relation+to+the+composition+of+plankton#0

Rees, A. P., Joint, I., & Donald, K. M. (1999). Early spring bloom phytoplankton-nutrient dynamics at the Celtic Sea shelf edge. *Deep-Sea Research Part I Oceanographic Research Papers*, *46*(3), 483–510. https://doi.org/10.1016/S0967-0637(98)00073-9

Richardson, P. L. (2007). Agulhas leakage into the Atlantic estimated with subsurface floats and surface drifters. *Deep-Sea Research Part I Oceanographic Research Papers*, *54*(8), 1361–1389. https://doi.org/10.1016/j.dsr.2007.04.010

Richardson, P. L., Lutjeharms, J. R., & Boebel, O. (2003). Introduction to the "Inter-ocean exchange around southern Africa". *Deep-Sea Research Part II Topical Studies in Oceanography*, *50*(1), 1–12. https://doi.org/10.1016/S0967-0645(02)00376-4

Rigg, G. M. (1995). *The hydrography and dynamics of rings adn eddies of the Agulhas current retroflection February-March 1987*. University of Cape.

Rubio, A., Blanke, B., Speich, S., Grima, N., & Roy, C. (2009). Mesoscale eddy activity in the southern Benguela upwelling system from satellite altimetry and model data. *Progress in Oceanography*, *83*(1–4), 288–295. https://doi.org/10.1016/j.pocean.2009.07.029

Santoro, A. E., Sakamoto, C. M., Smith, J. M., Plant, J. N., Gehman, A. L., Worden, A. Z., et al. (2013). Measurements of nitrite production in and around the primary nitrite maximum in the central California Current. *Biogeosciences*, *10*(11), 7395–7410. https://doi.org/10.5194/bg-10-7395-2013

Sarthou, G., Baker, A. R., Blain, S., Achterberg, E. P., Boye, M., Bowie, A. R., et al. (2003). Atmospheric iron deposition and sea-surface dissolved iron concentrations in the eastern Atlantic Ocean. *Deep-Sea Research Part I Oceanographic Research Papers*, *50*(10–11), 1339–1352. https://doi.org/10.1016/S0967-0637(03)00126-2

Schlitzer, R. (2016). Ocean Data view (ODV).

Schön, G. H., & Engel, H. (1962). Der Einfluß des Lichtes auf Nitrosomonas europaea Win. *Archiv Für Mikrobiologie*, *42*(4), 415–428. https://doi.org/10.1007/BF00409076

Schouten, M. W., De Ruijter, W. P. M., Van Leeuwen, P. J., & Lutjeharms, J. R. E. (2000). Translation, decay and splitting of Agulhas rings in the southeastern Atlantic Ocean. *Journal of Geophysical Research*, *105*(C9), 21913–21925. https://doi.org/10.1029/1999jc000046

Scott, B. D. (1981). Hydrological structure and phytoplankton distribution in the region of a warm-core eddy in the Tasman Sea. *Marine and Freshwater Research*, *32*(4), 479–492. https://doi.org/10.1071/MF9810479

Shiozaki, T., Ijichi, M., Isobe, K., Hashihama, F., Nakamura, K. I., Ehama, M., et al. (2016). Nitrification and its influence on biogeochemical cycles from the equatorial Pacific to the Arctic Ocean. *The ISME Journal*, *10*(9), 2184–2197. https://doi.org/10.1038/ismej.2016.18

Siegel, D. A., McGillicuddy, D. J., & Fields, E. A. (1999). Mesoscale eddies, satellite altimetry, and new production in the Sargasso Sea. *Journal of Geophysical Research*, *104*(C6), 13359–13379. https://doi.org/10.1029/1999jc900051

Sigman, D., Casciotti, K. L., Andreani, M., Barford, C., Galanter, M., & Böhlke, J. K. (2001). A Bacterial Method for the Nitrogen Isotopic Analysis of Nitrate in Seawater and Freshwater. *Analytical Chemistry*, *73*, 4145–4153.

Smart, S. M., Fawcett, S. E., Thomalla, S. J., Weigand, M. A., Reason, C. J. C., & Sigman, D. M. (2015). Isotopic evidence for nitrification in the Antarctic winter mixed layer. *Global Biogeochemical Cycles*, *29*(4), 427–445. https://doi.org/10.1002/2014gb005013

Smith, J. M., Casciotti, K. L., Chavez, F. P., & Francis, C. A. (2014). Differential contributions of archaeal ammonia oxidizer ecotypes to nitrification in coastal surface waters. *The ISME Journal*, *8*(8), 1704–1714. https://doi.org/10.1038/ismej.2014.11

Smith, S., Altieri, K. E., Mdutyana, M., Walker, D. R., Parrott, R. G., Gallie, S., et al. (2022). Biogeochemical controls on ammonium accumulation in the surface layer of the Southern Ocean. *Biogeosciences*, *19*(3), 715–741. https://doi.org/10.5194/bg-19-715-2022

Sohm, J. A., Hilton, J. A., Noble, A. E., Zehr, J. P., Saito, M. A., & Webb, E. A. (2011). Nitrogen fixation in the South Atlantic Gyre and the Benguela upwelling system. *Geophysical Research Letters*, *38*(16), L16608. https://doi.org/10.1029/2011GL048315

Spall, S., & Richards, K. J. (2000). A numerical model of mesoscale frontal instabilities and plankton dynamics—I. Model formulation and initial experiments. *Deep Sea Research Part I: Oceanographic Research Papers*, *47*(7), 1261–1301. https://doi.org/10.1016/s0967-0637(99)00081-3

Speich, S., Lutjeharms, J. R. E., Penven, P., & Blanke, B. (2006). Role of bathymetry in Agulhas Current configuration and behaviour. *Geophysical Research Letters*, *33*(23), 2–6. https://doi.org/10.1029/2006GL027157

Stern, M. (1965). Interaction of a uniform wind stress with a geostrophic vortex. *Deep-Sea Research and Oceanographic Abstracts*, *12*(3), 355–367. https://doi.org/10.1016/0011-7471(65)90007-0

Strickland, J. D., & Parsons, T. R. (1972). *A practical handbook of seawater analysis*. Fisheries Research Board of Canada. https://doi.org/10.2307/1979241

Sun, X., Ji, Q., Jayakumar, A., & Ward, B. B. (2017). Dependence of nitrite oxidation on nitrite and oxygen in low-oxygen seawater. *Geophysical Research Letters*, *44*(15), 7883–7891. https://doi.org/10.1002/2017GL074355

Sutka, R. L., Ostrom, N. E., Ostrom, P. H., & Phanikumar, M. S. (2004). Stable nitrogen isotope dynamics of dissolved nitrate in a transect from the north Pacific Subtropical Gyre to the Eastern Tropical North Pacific. *Geochimica et Cosmochimica Acta*, *68*(3), 517–527. https://doi.org/10.1016/s0016-7037(03)00483-6

The Ring Group. (1981). Gulf Stream cold-core rings: Their physics, chemistry, and biology. *Science*, *212*(4499), 1091–1100. https://doi.org/10.1126/science.212.4499.1091

van Aken, H. M., van Veldhoven, A. K., Veth, C., De Ruijter, W. P. M., Van Leeuwen, P. J., Drijfhout, S. S., et al. (2003). Observations of a young agulhas ring, astrid, during MARE in March 2000. *Deep-Sea Research Part II Topical Studies in Oceanography*, *50*(1), 167–195. https://doi.org/10.1016/S0967-0645(02)00383-1

Van Oostende, N., Fawcett, S. E., Marconi, D., Lueders-Dumont, J., Sabadel, A. J. M., Woodward, E. M. S., et al. (2017). Variation of summer phytoplankton community composition and its relationship to nitrate and regenerated nitrogen assimilation across the North Atlantic Ocean. *Deep-Sea Research Part I Oceanographic Research Papers*, *121*, 79–94. https://doi.org/10.1016/j.dsr.2016.12.012

Varela, M. M., Bode, A., Fernández, E., Gónzalez, N., Kitidis, V., Varela, M., & Woodward, E. M. S. (2005). Nitrogen uptake and dissolved organic nitrogen release in planktonic communities characterised by phytoplankton size-structure in the Central Atlantic Ocean. *Deep-Sea Research Part I Oceanographic Research Papers*, *52*(9), 1637–1661. https://doi.org/10.1016/j.dsr.2005.03.005

Villar, E., Farrant, G. K., Follows, M., Garczarek, L., Speich, S., Audic, S., et al. (2015). Environmental characteristics of Agulhas rings affect interocean plankton transport. *Science*, *348*(6237,1261447. https://doi.org/10.1126/science.1261447

Volk, T., & Hoffert, M. I. (1985). Ocean carbon pumps: Analysis of relative strengths and efficiencies in ocean-driven atmospheric CO_2 changes. *The Carbon Cycle and Atmospheric CO2: Natural Variations Archean to Present*, *32*, 99–110. Retrieved from http://www.scopus.com/inward/record.url?scp=0022222645%26partnerID=8YFLogxK%0Ahttp://www.scopus.com/inward/citedby.url?scp=0022222645%26partnerID=8YFLogxK

Walker, N. D., & Mey, R. D. (1988). Ocean/atmosphere heat fluxes within the Agulhas retroflection region. *Journal of Geophysical Research*, *93*(C12), 15473–15483. https://doi.org/10.1029/JC093iC12p15473

Wang, L., Huang, B., Laws, E. A., Zhou, K., Liu, X., Xie, Y., & Dai, M. (2018). Anticyclonic eddy edge effects on phytoplankton communities and particle export in the northern south China sea. *Journal of Geophysical Research: Oceans*, *123*(11), 7632–7650. https://doi.org/10.1029/2017JC013623

Ward, B. B. (2005). Temporal variability in nitrification rates and related biogeochemical factors in Monterey Bay, California, USA. *Marine Ecology Progress Series*, *292*, 97–109. https://doi.org/10.3354/meps292097

Ward, B. B. (2011). Measurement and distribution of nitrification rates in the oceans. In *Methods in enzymology* (Vol. 486, pp. 307–323). Academic Press. https://doi.org/10.1016/B978-0-12-381294-0.00013-4

Wasmund, N., Struck, U., Hansen, A., Flohr, A., Nausch, G., Grüttmüller, A., & Voss, M. (2015). Missing nitrogen fixation in the Benguela region. *Deep-Sea Research Part I Oceanographic Research Papers*, *106*, 30–41. https://doi.org/10.1016/j.dsr.2015.10.007

Weigand, M. A., Foriel, J., Barnett, B., Oleynik, S., & Sigman, D. M. (2016). Updates to instrumentation and protocols for isotopic analysis of nitrate by the denitrifier method. *Rapid Communications in Mass Spectrometry*, *30*(12), 1365–1383. https://doi.org/10.1002/rcm.7570

Welschmeyer, N. A. (1994). Fluorometric analysis of chlorophyll a in the presence of chlorophyll b and pheopigments. *Limnology and Oceanography*, *39*(8), 1985–1992. https://doi.org/10.4319/lo.1994.39.8.1985

Wolters, A. M., Jayawickrama, D. A., Webb, A. G., & Sweedler, J. V. (2002). NMR detection with multiple solenoidal microcoils for continuous-flow capillary electrophoresis. *Analytical Chemistry*, *74*(21), 5550–5555. https://doi.org/10.1021/ac025903k

Yool, A., Martin, A. P., Fernández, C., & Clark, D. R. (2007). The significance of nitrification for oceanic new production. *Nature*, *447*(7147), 999–1002. https://doi.org/10.1038/nature05885

Yoshimori, A., & Kishi, M. J. (1994). Effects of interaction between two warm-core rings on phytoplankton distribution. *Deep-Sea Research Part I*, *41*(7), 1039–1052. https://doi.org/10.1016/0967-0637(94)90017-5

Zakem, E. J., Al-Haj, A., Church, M. J., Van Dijken, G. L., Dutkiewicz, S., Foster, S. Q., et al. (2018). Ecological control of nitrite in the upper ocean. *Nature Communications*, *9*(1), 1206. https://doi.org/10.1038/s41467-018-03553-w

Zharkov, V., & Nof, D. (2008). Retroflection from slanted coastlines-circumventing the "vorticity paradox". *Ocean Science*, *4*(4), 293–306. https://doi.org/10.5194/os-4-293-2008